Geological Survey of Israel
Ministry of National infrastructures
Energy and Water Resources

Flowstone of Te'omim Cave, Israel: Characterization and Paleoclimate Trends in the middle Pleistocene transition

Yael Amid

Report GSI/39/2016

Jerusalem, December 2016

Geological Survey of Israel
Ministry of National infrastructures
Energy and Water Resources

Flowstone of Te'omim Cave, Israel:

Characterization and Paleoclimate Trends in the middle Pleistocene transition

Yael Amid

This thesis was submitted for the degree "Master" to the senate of the Hebrew University of Jerusalem.

The study was carried out under the supervision of:

Dr. Mira Bar-Matthews, Geological Survey of Israel.

Prof. Amos Frumkin, Cave Research Center, the Hebrew University of Jerusalem, Israel.

Report GSI/39/2016 Jerusalem, December 2016

Abstract

The Te'omim cave is an isolated karst cave located on the western slopes of the Jerusalem hills, approximately 20 km west of Jerusalem, at Nahal Hame'ara (Israel Grid 152049/126028). A wide array of vadose speleothems, such as flowstone, stalagmites and columns had accumulated in various parts of the main chamber, some of which producing thick accumulations of flowstone and large stalagmites. During a recent survey in the cave, a quarry was identified in the eastern part of the cave's main chamber. The quarry was dated by U-Th method using a flowstone deposited on the quarried surface after the cessation of quarrying, to the Middle Bronze Age (first half of the 2nd millennium BCE). The quarry is entirely within flowstone, composed of translucent, banded coarse crystalline calcite, suggesting that it was used in antiquity as a source of calcite 'Bahat' (alabaster). The term 'Bahat' is used in modern archaeological Hebrew literature to denote calcite-alabaster. Calcite-alabaster objects found in the southern Levant are commonly believed to be imported from Egypt. Ignoring the possibility of local calcite-alabaster sources, most researchers accepted the Egyptian source assumption formulated many years ago. However, calcite-alabaster quarries indeed existed in the southern Levant in at least two caves, Te'omim and 'Abud caves (approximately 11 km east of Shoham), most probably providing local workshops with an alternative source for this luxury material.

A cross section of flowstone ~3 m long, TM-2, was sawed from the wall of the quarry. It was selected where maximal thickness of relatively clean flowstone had accumulated, in order to identify the major sequence of the flowstone at the quarry. The upper 80 cm of TM-2 were studied in this research.

For dating, climatic and environmental change reconstruction purposes, $\delta^{18}O_c$ and $\delta^{13}C$ analyses are made at intervals of ~0.5-1.0 mm (459 drilled samples of TM-2 section). The top 10 cm of the section was previously dated using U-Th dating method. Dating of the older parts of the section was performed by applying the U-Pb and Paleomagnetic methods. TM-2 section was dated from ~1.3 Ma to ~50 ka. The U/Pb dating gave two ages of 1310 ±60 ka and 1350 ±120 ka, and the magneto-stratigraphy of this section gave five ages: 773ka, 1001ka, 1069ka, 1189ka and 1221ka. The isotopic profile was wiggle-matched with the isotopic record of LR04 benthic $\delta^{18}O_c$ stack. Fourteen isotopic events recorded in TM-2 isotopic profile, match MIS events ranging between 1316 ka and 773 ka. The average time interval between the major $\delta^{18}O_c$ peaks is about 40ka, matching the 41ka obliquity cycles that occurs until the beginning of the middle Pleistocene transition (MPT). Further bench marks are isotopic events with low $\delta^{18}O_c$ and high $\delta^{13}C$ which can be correlated with strong sapropel events in the Eastern Mediterranean Sea. Using the combined U-Pb ages, the magnetostratigraphy and wiggle-matching the isotopic events with benthic $\delta^{18}O_c$ stack and sapropel events suggests that the isotopic record of TM-2 reflects a long period of flowstone deposition since almost 1350ka. This record is the longest terrestrial paleoclimatic record at the Eastern Mediterranean region.

The isotopic profile demonstrates that during the MPT, there is a continuous flowstone growth during glacials and interglacials. The lower $\delta^{18}O$ values during glacials and interglacials of TM-2 section at the early Pleistocene compared with Soreq cave through the last 230ka indicate a temporal transition of climatic system during the MPT with symmetric glacial/interglacial cycles with 41 ka obliquity cycles changes by the end of

the MPT, at ~700 ka, to a highly nonlinear system dominated by ~100 ka periodicity with asymmetric glacial/interglacial cycles.

The petrography of the flowstone is characterized mainly by large columnar crystals, producing the typical 'Bahat' structure. In some cases, significant changes in the crystal habit follow changes in the isotopic trends.

Oxygen and carbon isotopic compositions of ‘Bahat’ archaeological artifacts samples from Egypt and Israel were also measured for comparing them to the isotopic composition of the TM-2 in order to gain information on the provenance of these artifacts. The isotopic composition of 'Bahat' archaeological artifacts samples from several archeological sites in Israel show that most of the 'Bahat' artifacts do not match the $\delta^{13}C$ - $\delta^{18}O$ combination of artifacts imported from Egypt. 'Bahat' artifacts from Umm el Umdan, Herodion, and Kotel match the isotopic composition of Te'omim Cave and could have been derived from Te'omim quarry.

Acknowledgements

I would like to express my special thanks of gratitude first and foremost to my supervisors: Dr. Miryam Bar-Matthews and Prof. Amos Frumkin for the interest they showed in my work, their guidance and their willingness to help at any given moment. I have learned a lot from them and profoundly benefitted from their knowledge and experience.

This work would not have been possible without the help and support of Dr. Avner Ayalon, who acted essentially as a supervisor of mine, and whose professional help, friendship, and general concern made things very enjoyable.

Thanks to Boaz Zissu, head of the archaeological expedition to the Teomim Cave, who provided administrative and financial support.

Special thanks go to the wonderful team from the Geochemistry Department at the Geological Survey of Israel (GSI): Tami Zilberman, Jonathan Keinan and Sergei Sladkevich for their help with performing the stable isotope measurements.

Many thanks to Miryam Bar-Matthews for the U-Th dating, to Ron Shaar and Yael Ebert from Hebrew University of Jerusalem for the magneto-stratigraphy dating and to Gideon Henderson at Oxford University, GB for the U-Pb dating.

Many thanks to Ayala Amir for providing the 'Bahat' Sample and for her help.

Thanks to my room colleagues from the GSI: Yuval Burstyn and Neta Shalev for sharing with me their knowledge and experience.

Many thanks to Gal Yas'ur for her great help with the research proposal.

Thanks to Lidia Grossovitch and Irit Gefen for their help with the polarizing optical microscope. Thanks to Iad Suaid for his help with the thin sections. Raanan Bodzin is thanked for his help with SEM analyses.

I wish to thank Anton Vaks and Ahuva Almogi-Labin for their help with relevant papers.

Funding for this project is provided by a grant no# 103/14 of the Israel Sciences Foundation (ISF). Israel Antiquities Authority and the Nature and Parks Authority provided sampling permits.

And last but not least thank you always to my family: Bnaya, Adi, Aner and Ivri, and to my parents Uzi and Yaffa Goldberg. You are always so understanding and loving and I could not make it without you.

Table of Content pp.

Table of Figures **pp**.

1 Background and previous studies

1.1 Te'omim Cave

1.1.1 Location and history of research

The Te'omim cave is an isolated karst cave located on the western slopes of the Jerusalem hills, approximately 20 km west of Jerusalem (Figure 1), at Nahal Hame'ara (Israel Grid 202049/726028). The cave was referred to as M˘ghâret Umm et Tûeimîn, 'the cave of the mother of twins', by local residents in the nineteenth century. The cave comprises a large chamber and one major side passage (Figure 2). Entry to the main chamber is sub-horizontal, with a 3 m vertical drop immediately inside the entrance, followed by a debris cone filling the chamber. The entrance was formed when subaerial denudation breached the edge of the cave, probably at the end of the Pleistocene, allowing human use of the cave during the Holocene, as evidenced from the archaeological finds (e.g. Zissu et al., 2011).

The first study of the cave was carried out by the Survey of Western Palestine team in 1873 (Conder and Kitchener, 1883, pp.148-149). The floor of the main chamber was partly excavated in the late 1920's by Neuville (1930) who published mainly the materials collected from a specific layer found in a small probe excavated near the entrance to the main chamber. This layer yielded various pottery sherds, lithics, bone and stone tools. In accordance with the available parallels at the time, Neuville attributed the finds to one period only, so-called "Bronze I tardif", which more or less parallels the more recent designation "Early Bronze Age". However, when examining the archaeological finds published, it is clear that the aforementioned layer contains mixed

materials from at least four different chronological periods: Neolithic, Chalcolithic (Ghassulian), Early Bronze and Intermediate Bronze Age. The fact that all these finds were collected from one spatial context points to the stratigraphic mixture common in natural caves. In addition, Neuville (1930) reported finds from the Middle and Late Bronze Age, Iron Age and the Roman and Byzantine periods.

In the early 1970's, G. Mann of the Society for the Protection of Nature in Israel surveyed the inner passage of the cave, and collected pottery, an oil lamp, and fragments of glass vessels which were attributed by Amos Kloner to the Roman and Byzantine periods (Mann, 1978).

A new archaeological-geological-speleological research project in the cave is taking place during the last decade by the Hebrew University, Bar-Ilan University, and the Geological Survey of Israel (e.g. Zissu et al., 2011). Among other finds, a flowstone quarry has been discovered (Frumkin et al., 2014), and is studied here within the framework of the new Teomim research project.

Figure 1: Location Map

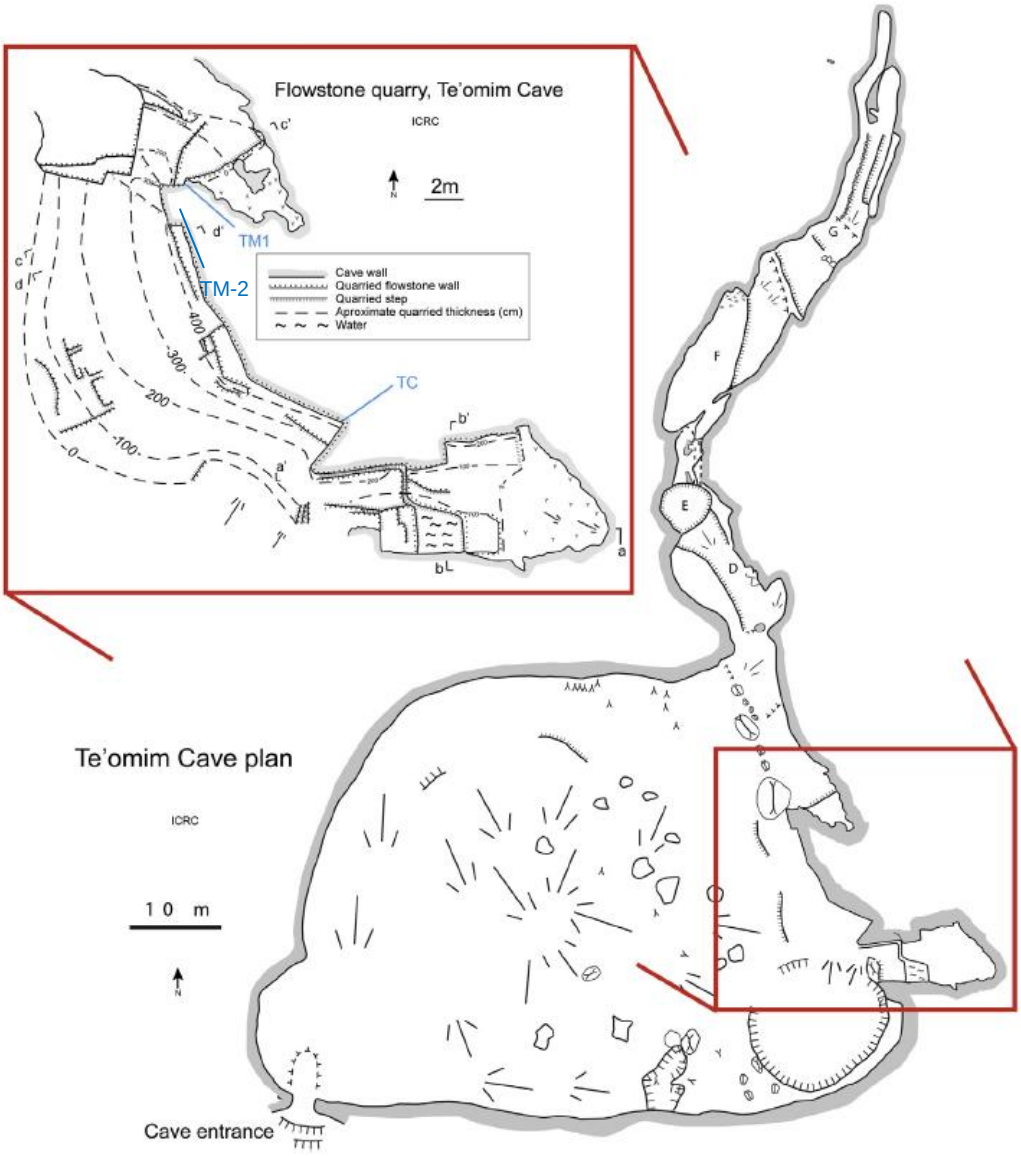

Figure 2: Plan of Te'omim Cave. The inset shows the main quarrying lines (abandoned quarry walls), as well as estimated iso-thickness lines (dashed) of quarried flowstone, after Frumkin et al. (2014).

1.1.2 Te'omim quarry

A wide array of vadose speleothems, such as flowstone, stalagmites and columns had accumulated in various parts of the main chamber, some of which producing thick accumulations of flowstone and large stalagmites. The flowstone had been deposited

by a sheet of water over a sloping surface under free-air conditions, prevailing since the cave emerged above the regional water table, millions of years ago (Frumkin and Fischhendler, 2005). During the recent survey in the cave, a quarry was identified in the eastern part of the cave's main chamber. Field examination and drilling revealed that the quarry is entirely within flowstone, composed of translucent, banded coarse crystalline calcite, suggesting that it was used in antiquity as a source of calcite-alabaster. The flowstone layering is partly seen in the quarried surfaces, while in other surfaces younger flowstone covers the wall. In many places there are signs of the cessation of quarrying scars or 'negatives' left on the quarry walls and floor after the removal of flowstone blocks (Figure 3). Few blocks of flowstone were never separated, due to fissures or defects in the bedrock. The quarry face, where quarrying had stopped, is up to 4 m high vertical wall of flowstone, underlain by additional flowstone, indicating that the original flowstone thickness was >4m. The quarry is 25 m long and up to 8 m wide (Figure 2). No indication for in situ production of vessels was observed during the archaeological survey of the cave (e.g. working tools, drills), and it seems reasonable to assume that vessel production took place in a proximate subaerial site. Water flow and dripping is an ongoing process on the quarried surfaces, where recent flowstone and other types of dripstone are still deposited today. The quarry was dated by U-Th of the flowstone deposited on the quarried surface after the cessation of quarrying. Such a date indicates the latest possible time of abandonment at this part of the quarry. Two drilled cores of flowstone, TC and TM1 were used. The oldest lamina (just above the quarried surface) of each core was dated (on 2012) by U-Th to 3426 ± 100 (2σ error) and 3585 ± 118 years for TC and TM1 cores respectively. Younger layers, four and one cm above the oldest

ones, yielded the ages 2704 ±102 and 3434 ±168 years respectively (Frumkin et al., 2014).

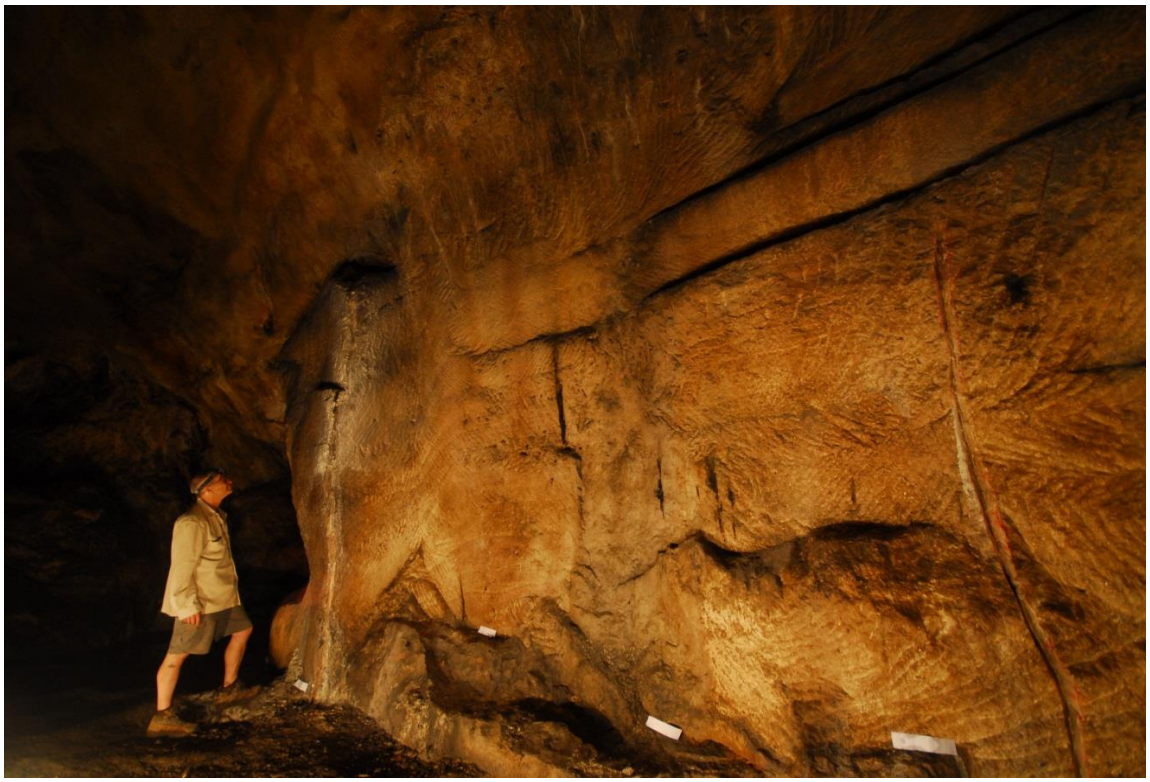

Figure 3: Te'omim cave quarry.

1.2 Speleothems formation

Speleothems usually form in karstic terrains with carbonate host rocks as a result of chemical reactions between rain water, soil and host rock (e.g. Richards & Dorale, 2003; McDermott, 2004). Rainwater percolating through the soil, results in water with high pCO_2 and low pH value. The high pCO_2 leads to formation of carbonic acid (equations 1 and 2):

1) $CO_{2(g)} \leftrightarrow CO_{2(aq)}$

2) $CO_{2(aq)} + H_2O_{(l)} \leftrightarrow H^+_{(aq)} + HCO_3^-{}_{(aq)}$

The weakly acidic water migrates through the carbonate host rock, dissolving it and absorbing trace elements, such as uranium, and becomes saturated in respect to calcium carbonate (equation 3):

3) $H^{+}_{(aq)} + HCO_3^{-}{}_{(aq)} + CaCO_{3(s)} \longleftrightarrow Ca^{2+}_{(aq)} + 2HCO_3^{-}{}_{(aq)}$

The water reaches the cave where, due to oversaturation relative to the cave pCO_2, it degasses – a process which results in calcite precipitation (equation 4):

4) $Ca^{2+}_{(aq)} + 2HCO_3^{-}{}_{(aq)} \longleftrightarrow CaCO_{3(s)} + CO_{2(g)} + H_2O_{(l)}$

Speleothems can continuously grow, but hiatuses are common, due to lack of water or changes in the fracture system above the cave.

1.3 Flowstone and calcite-alabaster

Calcitic flowstone is a secondary limestone, composed usually of the mineral calcite, formed by deposition from film flow of water under vadose (unsaturated) conditions (Ford and Williams, 2007), usually as a coarsely crystalline, translucent speleothem. Its attractive shelly translucent banding derives from the subsurface deposition environment, where low energy conditions promote the growth of large, clear crystals. In volume, it is the most common speleothem, often with m-thick deposits. Flowstone may be deposited at a rate of micrometers to mm per year, depending strongly on water flow rate and composition of the water and atmospheric CO_2. Flowstone (and closely-associated vein calcite) was often used in ancient times for the production of high-valued objects. In Egyptological studies it is commonly referred to as ‘alabaster’, a term derived from ‘alabastrites’, the ancient Roman name of this stone (Harrell, 1995). However, archaeological terminology related to this material is confusing, as it is alternately

referred to in the literature as Egyptian alabaster, onyx, calcite, (Egyptian) travertine, marble, and more.

Calcite-alabaster was commonly used in Egypt from Early Predynastic times (5th-millennium BCE; e.g. Lucas, 1930) until the end of the Roman period, ~400 CE, as well as in recent times (Harrell et al., 2007). In Egypt, calcite-alabaster was used to produce many kinds of ornamental and high-class objects. It was one of the most popular materials in Egyptian stone vessel working due to its aesthetic qualities: attractive coloring, translucency, ability to take a high polish, and softness (3 in Mohs scale), which made it easy to work with and inscribe upon. Its use was limited to ambient temperatures because it is not heat-retardant. In the southern Levant, the present-day areas of Israel, Jordan, Lebanon and Syria, calcite-alabaster objects first appeared sporadically during the Late Chalcolithic through the Early Bronze Age (late 5th to the 3rd millennium BCE; e.g. Amiran, 1970; Ussishkin, 1980). During the Middle and Late Bronze Age, calcite alabaster artifacts peaked in the region (e.g. Clamer, 1976, 2007; Caubet, 1991; Press, 2011). During these periods, calcite-alabaster artifacts in the Levant comprise mainly small vessels. Calcite-alabaster artifacts declined in number during the Iron Age, and eventually disappeared after the Roman Byzantine period. The term ‘Bahat’ is used in modern archaeological Hebrew literature to denote calcite-alabaster. Calcite-alabaster objects found in the southern Levant are commonly believed to be imported from Egypt (e.g. Clamer, 1976; Ebeling, 2001; Press, 2011). Ignoring the possibility of local calcite-alabaster sources, most researchers accepted the Egyptian source assumption formulated many years ago (Ben-Dor, 1945). However, the Egyptian provenance assumption is not taken for granted by all researchers. Lilyquist (1996) noted that only

"few of the vessels assigned to Egypt being displayed in various cities of the Levant seemed unquestionably Egyptian in material, shape and detail". Lilyquist also mentioned examples of geological deposits in the Levant, suggesting that some of these could potentially be quarried for calcite-alabaster, but she brings no example of such quarries. Sparks (2007) has acknowledged the existence of potential calcite-alabaster sources in the Negev and Sinai deserts, without evidence of quarrying, but does not mention such deposits in the inhabited parts of the southern Levant. Sparks (2007, p. 160) noted also that "The main issue therefore becomes whether these sources are suitable for manufacturing stone vessels and whether it is possible to demonstrate knowledge or exploitation of them during the period under review", referring to the southern Levant.

Frumkin et al. (2014) show that calcite-alabaster quarries indeed existed in the southern Levant in at least two caves, Te'omim and 'Abud (approximately 11 km east of Shoham), most probably providing local workshops with an alternative source for this luxury material. They employed U/Th age dating to constrain the absolute date of these quarries, succeeding in one of the cave quarries. This age-dating is supported by conventional archaeological methods.

1.4 Paleoclimate

1.4.1 Marine isotope stages

Marine isotope stages (MIS), are alternating warm and cool periods in the Earth's paleoclimate, as deduced from oxygen isotope of benthonic foraminifera from deep sea core samples.

Oxygen isotope records obtained by analysis of benthic foraminifers from deep-sea cores in the Caribbean were divided by Emiliani (1955) into marine isotopes stages. Shackleton

and Opdyke (1973) provided evidence that the $\delta^{18}O_c$ record is dominated by the effect of changes in the oxygen isotopic composition of the global ocean and therefore that the isotope stages could be used as a means to create a global stratigraphic framework for marine sediment. Working backwards from the Holocene, which is MIS 1 in the scale; stages with even numbers have high $\delta^{18}O_c$ and represent cold glacial periods, while the odd-numbered stages are troughs in the $\delta^{18}O_c$, representing warm interglacial (or interstadial) intervals.

For the description of Quaternary marine sediments this scheme is almost universally applied, although the means by which it is applied varies; Prell et al. (1986) recommend the use of ‘‘events’’ (isotopic extremes) rather than boundaries (transitions between isotope stages) for applying the formal oxygen isotope stratigraphy (and associated timescale) to a core. At 2005, Lisiecki & Raymo published 5.3-Ma stack (the ‘‘LR04’’ stack) of benthic $\delta^{18}O_c$ records from 57 globally distributed sites aligned by an automated graphic correlation algorithm (Figure 4).

Numerous investigations have shown that the earth's climate responds linearly, to variations in the earth's orbital geometry (e.g. Hays el al, 1976; Komintz and Pisias, 1979). Since this climate response is continuously recorded in deep sea sediments by climatically sensitive parameters (as $\delta^{18}O_c$) the orbital\climate link provides possibility for establishing geochronology (Martinson at al, 1987). Indeed, the MIS data matches the astronomical data of Milankovitch cycles of orbital forcing or the effects of variations in insolation caused by cyclical slight changes in the eccentricity, obliquity (tilt of the earth's axis of rotation), and precession .

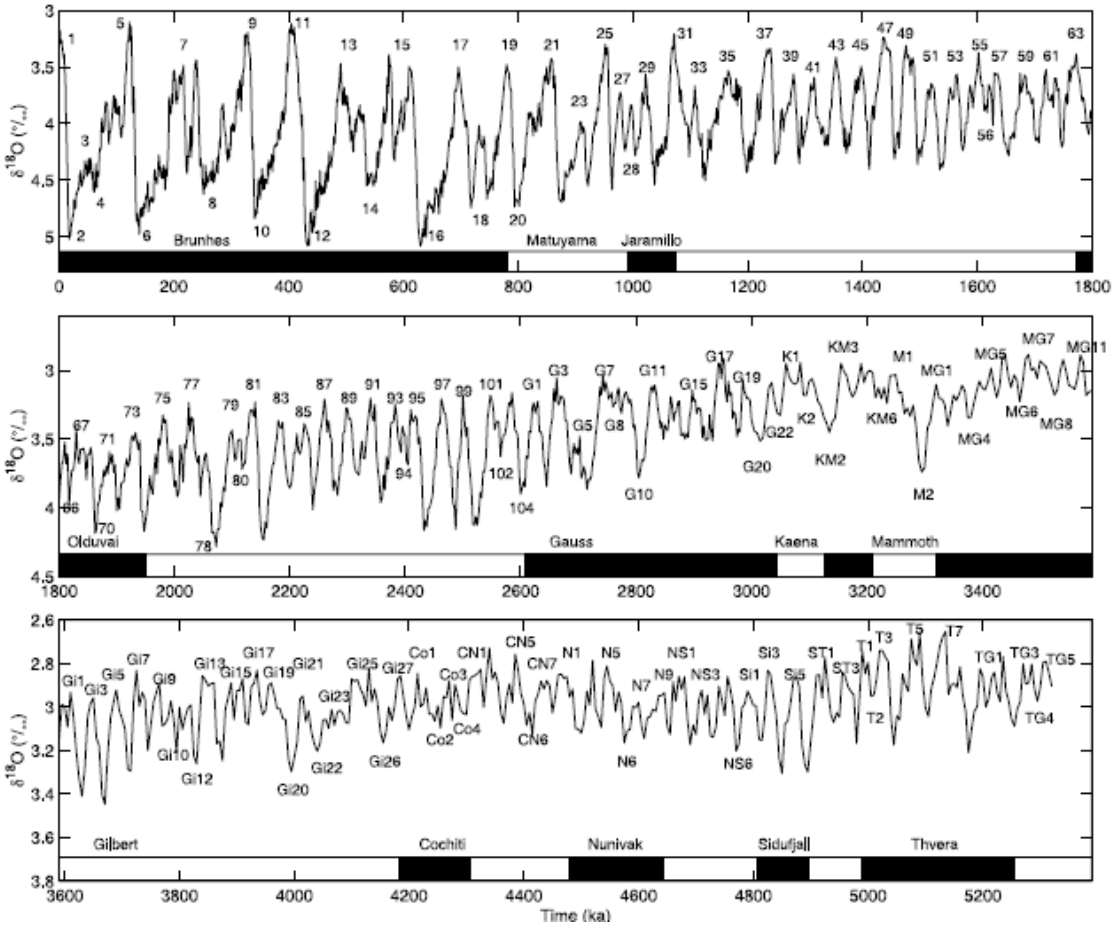

Figure 4: The LR04 benthic $\delta^{18}O$ stack constructed by the graphic correlation of 57 globally distributed benthic $\delta^{18}O$ records. Marine isotopes Stages compared with paleomagnetic time scale, after Lisiecki and Raymo, 2005. Black bars indicate normal polarity and white bars is reversed polarity.

1.4.2 Middle Pleistocene Transition (MPT)

The last stage in the transition from early to mid-Pleistocene is known as the Middle Pleistocene Transition (MPT), starting at ~1.25 Ma and ending around 0.7 Ma.

This transition (Figure 5) represents a major shift in the earth's history since the first ice sheets started accumulating in the northern hemisphere ~2.6 Ma. Ice-sheet growth linearly followed the 41 ka obliquity cycles until the beginning of the MPT. By the end of the MPT, at ~700 ka, this mode shifted to a highly nonlinear system dominated by ~100

ka. periodicity (Lisiecki and Raymo, 2005; Clark et al., 2006) with asymmetric glacial/interglacial cycles (Figure 5). Large-scale ice-sheet growth in the northern hemisphere coincides with the onset of MPT, representing a fundamental change in ice-sheet dynamics. The change was attributed to an increase in ice-sheet thickness rather than in areal extent (Clark et al., 2006; Sosdian and Rosenthal, 2010). The first major glaciation, indicated by a substantial increase in ice volume, predates the end of the MPT, occurring at ~880 ka during glacial stage 22, with increasing severity and duration of this cold stage compared with earlier glacial stages (Figure 5). Later on, between ~850 ka and ~750 ka there were notable minima in summer solar forcing at 65°N and markedly smaller amplitude in the ~23 ka, ~100 ka, and ~400 ka orbital bands (Figure 5).

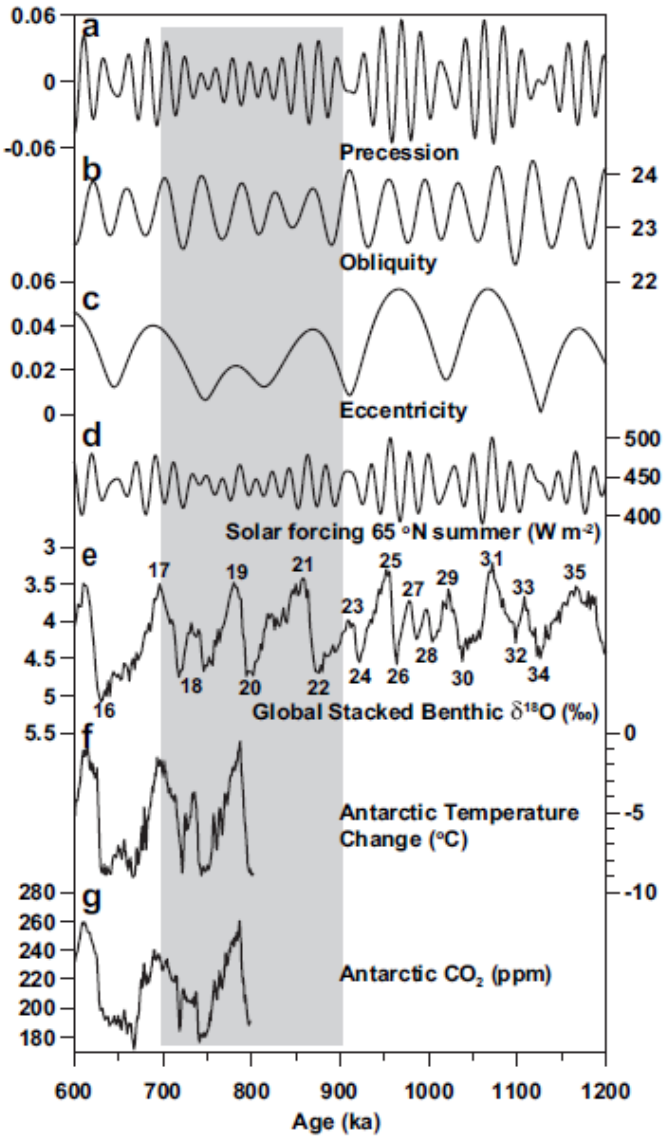

Figure 5: Precession (a), Obliquity (b) and Eccentricity (c) orbital cycles and summer solar forcing at 65°N (d) following Berger and Loutre (1991), compared with the global stacked $\delta^{18}O$ benthic foraminifera record (e) of Lisiecki and Raymo (2005), the numbers are Marine isotopes Stages. Compilation of temperature anomaly (f) and CO_2 concentration records (g) between 810 and 600 ka in Antarctic EPICA Dome C ice core following Jouzel et al. (2007) and Lüthi et al. (2008). The vertical gray bar defines the latest part of the MPT, between 900 and 700 ka.

1.4.3 Sapropels events

Sapropel is a term used to describe dark-coloured marine sediments that are rich in organic matter. Organic carbon concentrations in sapropels commonly exceed 2% in weight.

The sapropel occurrences in the marine sequences over the entire Eastern Mediterranean (EM) are considerable; with the resolution that can be obtained from isotope studies, groups of sapropels occurred simultaneously over the entire basin (Emeis at al., 1998). Studies on the geochemistry and facies of sapropels agree that anoxic conditions favored preservation of organic matter in sapropels, caused the enrichment of trace metals associated with sapropels, and helped preserve primary sedimentary structures. All evidence is consistent with elevated flux of organic matter and associated elements during sapropel events.

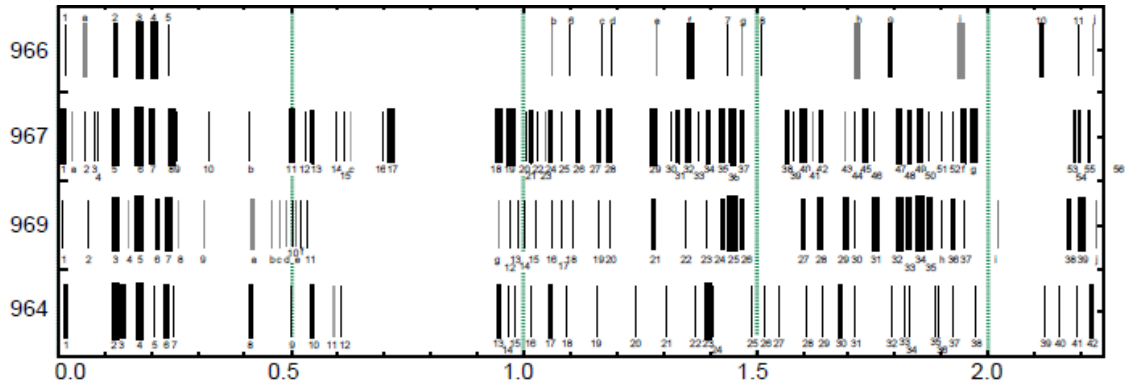

Figure 6: Compilation of sapropel occurrences through time at Sites 964, 969, 967, and 966 (in the Mediterranean Sea) for the last 2.25 m.y. Gray bars denote sapropel ghosts. Bar width is an indication of sapropel thickness (Emeis at al, 1998).

Lower $\delta^{18}O_{speleothems}$ of the EM surface is associated with sapropel formation in the EM (Bar-Matthews et al., 2000), as a result of freshening of the Mediterranean sea surface due to increasing input of rainfall, glacial meltwater from European-Black Sea systems,

and Nile River and rivers from the Sahara discharge, associated with increased African monsoon rains (for review see Bar-Matthews, 2014). The climatic conditions during the sapropel events are also reflected in the terrestrial record. $\delta^{13}C$ values of Soreq Cave speleothems present more complicated features. During most of the interglacials, $\delta^{13}C$ values range between -13 and -10‰, typical of C3-dominated vegetation, but during MIS 5e (128-120 ka) and during the early Holocene (9.4 and 7.0 ka), $\delta^{13}C$ values are extremely high, rising to ~0‰ and ~ -5.0‰ at MIS 5e and early Holocene respectively. The very high $\delta^{13}C$ during these intervals are coupled with the very low $\delta^{18}O$. Bar-Matthews et al. (2000) interpreted this coupling as reflecting deluge events, where $\delta^{13}C$ cannot reflect the soil-CO_2 composition due to high water flushing to the cave that result in isotopic composition approaching the surrounding dolomite host rock. Evidence for this process is provided by the large amount of detrital material incorporated in the Soreq Cave speleothems during these time intervals (Ayalon et al., 1999), and the sharp drop in the concentrations of Sr, Ba, and U, and in the ratios of $(^{234}U/^{238}U)_0$ and $^{87}Sr/^{86}Sr$, which reflect enhanced weathering of the host-rock (Kaufman et al., 1998; Ayalon et al., 1999; Bar-Matthews et al., 2000).

Bar-Matthews et al. (2000, 2003) estimated that rainfall during these events could have been 20%-70% higher than present-day amounts. Alternatively, Frumkin et al. (2000) suggest that the high $\delta^{13}C$ during 128-120 ka can be the outcome of unstable, dry and warm conditions, loss of vegetation, and erosion of the soil cover. This hydrologic regime is consistent with irregular high water flushing events: flash-floods are potentially more common under scarce vegetation cover. Such fluctuating dry-hot intervals could have

enhanced forest fires, followed by rapid soil erosion; eventually leading to abrupt changes and high $\delta^{13}C$. The high Soreq cave pool levels during the 128-120 ka interval indicate that some flash-floods were frequent enough to keep the pools full, long enough for calcite deposition. Enhanced rainfall over the Mediterranean basin during sapropel events is evident from the similar salinity trend in the entire Mediterranean basin (Kallel et al., 1997) and from combined biotic and abiotic proxies in the Yammouneh basin (Lebanon) (Gasse et al., 2015). The extreme arid region of northeast Africa experienced episodes of considerable increase in rainfall at this time associated with EM rainfall front, coinciding in time with increased African monsoon activity (Vaks et al., 2010). Less wet conditions developed during the intervals of sapropels S3 and S4 (~109-107 ka to 104-100 ka and 86-83 ka, respectively). In general, the speleothem evidence reflects highly unstable and erratic conditions during these deglacial/interglacial transitions.

During interglacial substages, between sapropel events (e.g. MIS 5.2, 5.4, 7.2, 7.4 etc.,) the $\delta^{18}O_{Cc}$ are higher by ~2-3‰, reflecting change in the $\delta^{18}O$ of the source water and increased aridity in the region. The increased aridity is also evident from the marine record indicating aeolian deposits replacing fluvial Nilotic contribution (Almogi-Labin et al., 2004, 2009).

1.5 Paleoclimate reconstruction using stable isotopes in speleothems

1.5.1 Oxygen isotopic composition

Speleothems are used as archives providing information related to environmental conditions, which are monitored using their isotopic and chemical composition. Once the chronology and growth rate of the speleothem are determined, a detailed climatic reconstruction can be made, using $\delta^{18}O_c$ and $\delta^{13}C$ values (e.g., McDermott, 2004). The

fractionation of $^{18}O/^{16}O$ between water and calcite during the precipitation of the speleothems depends on the temperature in the cave and the $\delta^{18}O_w$ of the cave water. The $\delta^{18}O$ of the cave water is closely related to the isotopic composition of the rainwater (Ayalon, et al., 1998), and the cave temperature reflects average annual temperature in the area. $\delta^{18}O_w$ of rainwater is a function of various parameters, including the isotopic composition of the source, temperature, distance from the rainfall source and the amount of precipitation also referred as the "amount effect" (Bar-Matthews et al., 2003; Kolodny et al., 2005), latitude and altitude. The "source effect" is significant on the long-term behavior of isotopic reservoirs of the east Mediterranean region: Speleothem $\delta^{18}O_c$ is strongly influenced by the marine reservoir that contributes its vapor to rain formation. Short-term variations in the isotopic composition of rainfall are dominated by the amount effect and the temperature. Periods of low $\delta^{18}O_c$ values in Soreq Cave speleothems were interpreted as related to warming, and increase in the rainfall amount (Bar-Matthews, et al., 2000). High values of $\delta^{18}O_c$ in Soreq Cave speleothems are related to global cooling episodes, such as Heinrich events and the LGM.

1.5.2 Carbon isotopic composition

The $\delta^{13}C$ values of cave waters reflect the contribution of the dolomitic host rock and of soil-CO_2, CO_2 degassing and carbonate precipitation (e.g. Frumkin, et al., 2000; Genty & Massault, 1999; Bar-Matthews, et al., 1996). Soil-CO_2 is a major source of carbon to the speleothems, and $\delta^{13}C$ of soil-CO_2 gas mostly depends on the type of photosynthesis pathway and also on the intensity of biogenic activity and deserts tend. Thus, $\delta^{13}C$ fluctuations shown in speleothems may reflect changes in the vegetation type in the cave area. There are two major photosynthetic pathways: C_3 and C_4. The C_3 pathway is usually

used by trees, shrubs and cool climate herbs. The C_4 pathway is used by warmer climate adapted grasses and herbs. Average $\delta^{13}C$ values of C3 vegetation is ~ -27‰, and of C_4 is ~ -12‰ (Smith and Epstein, 1971; Deins, 1980). The expected range of $\delta^{13}C$ in carbonates in regions dominated by C_3 plants is -14 to -6‰ whereas those dominated by C_4 plants range between -6 to +2‰ (Bourdon, et al., 2003).

Other factors controlling the carbon isotopic composition are the presence or absence of soil cover, intensity of carbonate host-rock dissolution and water–rock interactions in the unsaturated zone (e.g., Bar-Matthews et al., 1996; Hendy, 1971; Genty et al., 2001; Frumkin, et al., 2000). Environmental parameter such as water stress, high temperature and CO_2 level may affect the plant $\delta^{13}C$ value by an increase in the range of 2-4‰ (e.g., Ehleringer and Cooper, 1988; Tieszen, 1991)

1.6 Petrography

Experiments have demonstrated that crystal morphology and growth mechanisms yield much information on the physicochemical parameters of the parent fluid (Sunagawa, 1987). Crystals form when there is departure from equilibrium, which, for sparingly soluble salts (such as calcium carbonate), is the degree of supersaturation. As supersaturation increases, crystal habits are expected to change from prismatic to spherulitic (Boistelle, 1982). Kim and O'Neil (1997) demonstrated that nonequilibrium isotope fractionation in calcite occurs when crystals grow at high supersaturation resulting in kinetic fractionation. Departure from equilibrium growth, therefore, may influence both the form (habit) and the isotopic properties of calcite crystals.

Gonzalez et al. (1992) illustrated that spelean calcite crystal habit is controlled by supersaturation, and fabrics are controlled by flow rate. Changes in calcite fabrics and crystal habits, therefore, have the potential to provide a record of supersaturation and changes in water availability through time (Szabo et al. 1994).

Crystal habits, however, are not controlled solely by the degree of supersaturation but also by other factors such as crystal structure (Burton et al.1951), the presence of foreign ions, and the kinetics of growth processes (Prieto et al. 1981).

The combination of different factors such as drip rate, supersaturation, impurity content, and, possibly, Mg/Ca ratio of the parent waters seemingly control the development of columnar, fibrous, microcrystalline, dendritic, and calcareous fabrics in speleothems. Most of these factors are detectable through petrographic observations. Secondary changes, such as neomorphism or transformation also impact speleothem preservation of climate signals and are, potentially, detectable by petrographic observations also.

Commonly, speleothems are mineral aggregates formed in voids (caves) – only a few speleothems consist of single crystals (Frisia, 2000). The fabric is, thus: "a geometric picture formed by the dividing surfaces of the separate mineral individuals which form the mineral aggregate" (Stepanov, 1997).

For example, columnar fabric proper has been interpreted as forming at relatively low supersaturation, regular flow, negligible presence of "foreign ions" (Frisia, 2000) and "feathered" like, columnar may form because of the presence of magnesium, sulphate, or microbes (Folk, 1965). Likewise, large detritus free crystals are common during glacial periods when water dripping was more continuous and slow compared with early Holocene (Bar-Matthews et al., 1997).

1.7 The use of stable isotopes for identifying provenance of ancient vessels

To determine the provenance of artifacts, each potential source area must be "finger-printed" and a database built up of sources. The distinctive fingerprints can base on petrographic, magnetic, geochemical or any other distinguishing physical characteristics of the material.

The most widely used procedure today for identification of white marbles involves a combination of microscope and C-O stable isotope analyses (Gorgoni et al, 2002). As early as the beginning of the 1970s, Craig and Craig (1972) highlighted the importance of the carbon and oxygen isotopic signature for provenance study of archeological white marbles, and proposed the first comparative data bank in the form of correlation clusters. Over the following years, the first database was developed and detailed by several researchers (Manfra et al, 1975; Hertz, 1986). This progressive implantation proceeded in two directions: 1. By creating sets of reference data for new supply areas of known or

potential archeological interest never previously considered and 2. By improving and detailing the database for the most important marbles of classical antiquity.

For example, a study has been made of $\delta^{18}O_c$ and $\delta^{13}C$ variations in Greek marbles from the ancient quarry localities of Naxos, Paros, Mount Hymettus, and Mount Pentelikon. Parian, Hymettian, and Pentelic marbles can be clearly distinguished by the isotopic relationships; Naxian marbles fall into two groups characterized by different oxygen-18/oxygen-16 ratios. Ten archeological samples were also analyzed; the isotopic data indicate that the "Theseion" is made of Pentelic marble and a block in the Treasury of Siphnos at Delphi is probably Parian marble (Craig, 1972).

Here we shall use, in a similar way, stable isotopes of oxygen and carbon for preliminary identification of the provenance of some ‘bahat’ artifacts.

2 Aims and research goals

This research has three main goals:

(1) To identify the character of local calcite-alabaster raw material, based on petrographic and isotopic parameters of TM-2 flowstone section from the quarry at the Te'omim cave. These parameters will be used to determine whether shifts in the isotopic composition are associated with change in crystal growth.

(2) To date the entire studied section of TM-2 using paleomagnetic tools, U-Pb and U-Th methods and by comparing isotopic events with the global stacked $\delta^{18}O_c$ benthic foraminifera record, timing of magnetic reversals and sapropel events. The paleo environment of the southern Levant during the growth period of TM-2 will be deduced

from the analysis of oxygen and carbon stable isotope values. This will shed light on long-range terrestrial climate change and its extreme values.

(3) To compare the isotopic composition of the TM-2 to the isotopic composition of archeological artifacts from several locations in order to add information on the provenance of archaeological artifacts that were produced from this site as opposed to alternative sources.

As mentioned above, calcite-alabaster objects found in the southern Levant are commonly believed to be imported from Egypt (e.g. Clamer, 1976; Ebeling, 2001; Press, 2011). Ignoring the possibility of local calcite-alabaster sources, most researchers accepted the Egyptian source assumption formulated many years ago (Ben-Dor, 1945). In this research petrographic and isotopic characteristics of the calcite-alabaster will enable the characterization of the local alabaster, that were quarried from the local flowstone quarry in the Te'omim Cave.

3 Methodology

3.1 Flowstone sampling in the cave

A cross section of flowstone ~3 m long, TM-2, was sawed by Makita grinder saw from the wall of the Te'omim cave quarry (Figure 7, Figure 8). It was selected where maximal thickness of relatively clean flowstone had accumulated, in order to identify the major sequence of the flowstone at the quarry. Additional 'new' flowstone deposited on the quarried surface was also sampled. The upper 80 cm of TM-2 section that used for this study was separated to 7 parts, TM2-1 is the upper one and TM-2-7 is the lowest (Figure 8).

Figure 7: Sawing the sample from the wall of Te'omim Cave quarry.

Figure 8: The entire TM-2 sampled section.

Figure 9: Image section TM2-2.

3.2 Dating

The top 10 cm of the section (~80 cm) was previously dated using uranium-thorium (U-Th) dating method. Because several discontinuities were observed in the top 10 cm, it was not possible to estimate the growth rate of the entire section from the growth rate of the top 10 cm. The age model was performed by using the U-Pb and the Paleomagnetic ages, together with wiggle matching the isotopic record to the LR04 benthic $\delta^{18}O_c$ stack. The sapropel events were identified in the speleothems record by extremely low $\delta^{18}O_c$ and high $\delta^{13}C$ as was found to late Pleistocene speleothems from Soreq, Peqi'in and Jerusalem caves (Bar-Matthews et al., 2003; Frumkin et al., 1999) which help to constrain the chronology of the older part of the section.

The dating methods are described below:

3.2.1 Uranium-Thorium dating

U-Th dating of the top 10 cm of the flowstone section was performed at the geochemistry lab of the Geological Survey of Israel (GSI) by Mira Bar-Matthews, using a Nu Instruments Ltd (UK) Multi-Collector-Inductively-Coupled-Plasma-Mass-Spectrometer (MC-ICP-MS) equipped with 12 Faraday cups and 3 ion counters. The location of the dated samples was at 2, 3, 4 and 5 cm distance from the top of the section. U-Th dating was carried out following the method described in detail by Vaks et al. (2006) and Grant et al. (2012). Ages of flowstone section was calculated according to the following equation (Kaufman et al., 1998):

$$\left(\frac{^{230}Th}{^{234}U}\right)=\left(\frac{^{238}U}{^{234}U}\right)\cdot(1-e^{-\lambda_{230}t})+\left(1-\left[\frac{^{238}U}{^{234}U}\right]\right)\cdot\left(\frac{\lambda_{230}}{\lambda_{230}-\lambda_{234}}\right)\cdot\left[1-e^{(-\lambda_{230}-\lambda_{234})t}\right]$$

Where t is the age, λ_{230} and λ_{234} are the decay constants of ^{230}Th and ^{234}U, respectively, and all ratios represent activity ratios. The ages were calculated using Newton-Raphson iteration, which gives the final age and the analytical error (±2σ; two standard errors of the mean). Age correction methods were applied as needed (Kaufman, 1993; Hershkovitz et al., 2015).

3.2.2 Magneto-stratigraphy

Magneto-stratigraphy method works by collecting oriented samples at measured intervals throughout the section, in order to represent all of it. The samples are analyzed to determine their characteristic remnant magnetization (ChRM), that is, the polarity of Earth's magnetic field at the time a stratum was deposited. Samples are first analyzed in their natural state to obtain their natural remnant magnetization (NRM). The NRM is then stripped away in a stepwise manner using thermal or alternating field demagnetization techniques to reveal the stable magnetic component.

Magnetic orientations of all samples from a site are then compared and their average magnetic polarity is determined with directional statistics. The latitudes of the Virtual Geomagnetic Poles from those sites determined to be statistically significant are plotted against the stratigraphic level at which they were collected. These data are then abstracted to the standard black and white magnetostratigraphic columns in which black indicates normal polarity and white is reversed polarity (Figure 10).

To locate the magnetic reversals in the time scale, at least one age obtained from another dating method is needed. With the aid of the independent age, the local magnetostratigraphic column is correlated with the Global Magnetic Polarity Time Scale (GMPTS) (Singer, 2014).

Oriented cores, 1'' in diameter were drilled in the section using electrical drill. The cores were sliced in the lab to smaller 1'' length specimens. Paleomagnetic stepwise demagnetization experiments were carried out in the paleomagnetic laboratory of the Institute of Earth Sciences, the Hebrew University of Jerusalem by Ron Shaar and Yael Ebert. Measurements were carried out using a 3-axis 2G cryogenic magnetometer with integrated Alternating Field (AF) demagnetization unit. Each specimen underwent multiple demagnetization steps at progressively increased field up to 90 mT to determine the paleomagnetic polarity.

3.2.3 Uranium-Lead dating

The method Uranium-Lead (U-Pb) chronology is usually applies to two U-Pb decay systems:

(1) $^{206}Pbm = {}^{206}Pbi + {}^{238}U(el_{238}t - 1)$

(2) $^{207}Pbm = {}^{207}Pbi + {}^{235}U(el_{235}t - 1)$

Where "m" refers to the measured amount of an isotope at present, "i" to its initial concentration, "l" is the decay constant for the appropriate isotope, and "t" is the time elapsed from initial conditions to the present. Uranium-lead dating is usually performed on the mineral zircon ($ZrSiO4$), but also been applied to other minerals such as calcite/aragonite and other carbonate minerals. The two U-Pb dates obtained from ^{238}U and ^{235}U have different half-lives, so if the dates obtained from the two decays are in agreement this adds confidence to the date.

Flowstone samples from Te'omim cave were U-Pb dated by Gideon Henderson at Oxford University, GB.

3.3 Oxygen and carbon isotopic composition

For climatic and environmental change reconstruction purposes, $\delta^{18}O_c$ and $\delta^{13}C$ analyses are made on 0.35-0.5 mg samples, obtained by drilling at intervals of ~0.5-1.0 mm and put in glass vials. Dry phosphoric acid (100%) is added to the top of the vials, which are placed in a horizontal position to avoid reaction with the carbonate. The samples are flushed with pure helium gas for 10 minutes in order to remove all atmospheric CO_2, and only then the vials are turned to vertical position to allow the phosphoric acid to react with the powder of the drilled samples dissolving the carbonate, and forming CO_2. The CO_2 is measured using a Delta V mass spectrometer with a Gas Bench automatic sampler in order to measure $\delta^{18}O_c$ and $\delta^{13}C$. All $\delta^{18}O_c$ and $\delta^{13}C$ values were calibrated against the international standard NBS-19, and are reported in permil (‰), relative to the VPDB standard

3.4 Oxygen and carbon isotopic composition of 'Bahat'

Oxygen and carbon isotope composition of ‘Bahat’ (alabaster) archaeological artifacts samples from Egypt and Israel were measured using the same technique described above. The 'Bahat' artifacts and their characteristics were supplied by Ayala Amir who studied the provenance of these objects for her MSc thesis, using other methods (e.g., trace elements, Sr isotopic composition). The description of each 'Bahat' samples is given in the supplementary section.

3.5 Optical microscopy

13 thin sections 30μm thick were taken lengthwise the TM-2 section. These thin sections were examined using polarization optical microscope Olympus BX50 in the GSI in order to determine their crystal growth habit and fabric.

4 Results

4.1 Dating

4.1.1 U-Th dating

U-Th dating of five samples from the top of the section yielded ages of ca. 53.1 ± 1.2 ka, 60.2 ± 0.8 ka, 109.4 ± 1.3 ka, and 488 ± 87 ka (Figure 10).

4.1.2 Magneto-stratigraphy

Figure 10 displays the TM-2 section and the location of the 26 samples taken for the magneto-stratigraphy dating.

The first reversal commonly dated to 773 ka occurs at about 10 cm from the top of the section. Comparison with the isotopic profile (see paragraph 4.2) suggests that the reversal point can be placed where isotopic measurement no. 100 was performed (Fig. 11).

4.1.3 U-Pb dating

Eight samples were dated U-Pb dating method. The sample powders were taken from the samples collected for paleomagnetic study, and are numbered with the same numbers as marked in Fig. 10. The results are as follows:

1. **Samples 1 and 6**: Contain high concentration of Pb and thus could not give reliable U-Pb age. Based on their $^{234}U/^{238}U$ ratio, their age is estimated at about 1000 ka.
2. **Samples 8, 12, 15:** located close to each other, gave an age of 1300 ka with error of ±60-120 ka.
3. **Sample 16:** Probably not a closed system.

4. **Sample 22:** Two replicates fail to give a good spread of U/Pb value, but fall close to data obtained for samples 8, 12, 15, suggesting a similar age of ~ 1300 ka. Age calculated based on the $^{234}U/^{238}U$ ratio, indicate a slightly older age of ~1450 ka.

5. **Sample 25**: Probably not a closed system.

The two ages that are marked below (~1300ka; Figure 10) are the ages from samples 8, 12, 15 and 22.

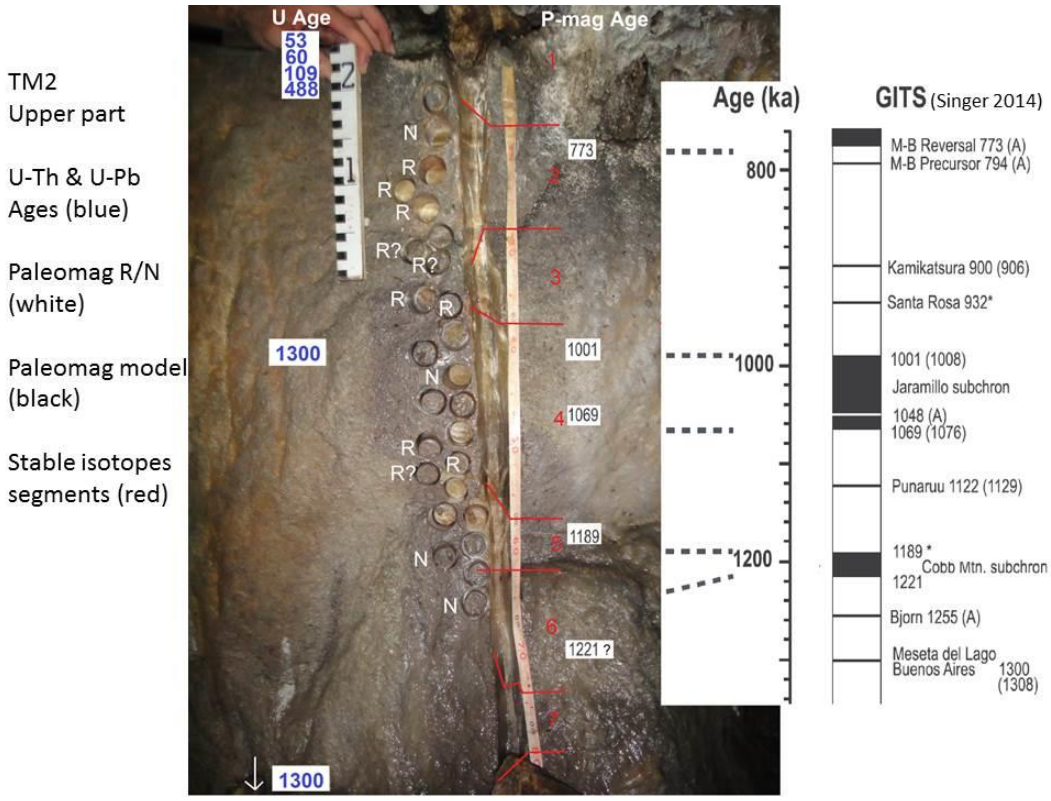

Figure 10: Dating results of TM-2 section: Ages from U/Th (Bar Matthews, 2014, unpublished) and U/Pb in ka (courtesy Henderson, 2016, unpublished) are marked in blue, and magneto-stratigraphic results, R-reversal in black and N- normal in white (courtesy Shaar, 2015, unpublished). Magneto-stratigraphic time scale is according to Singer (2014) and marked in black on the right. The suggested correlation with magneto-stratigraphic results is indicated by dashed lines.

4.2 Isotopic record

Figure 11 presents the $\delta^{18}O_c$ and $\delta^{13}C$ profiles of TM-2 section:

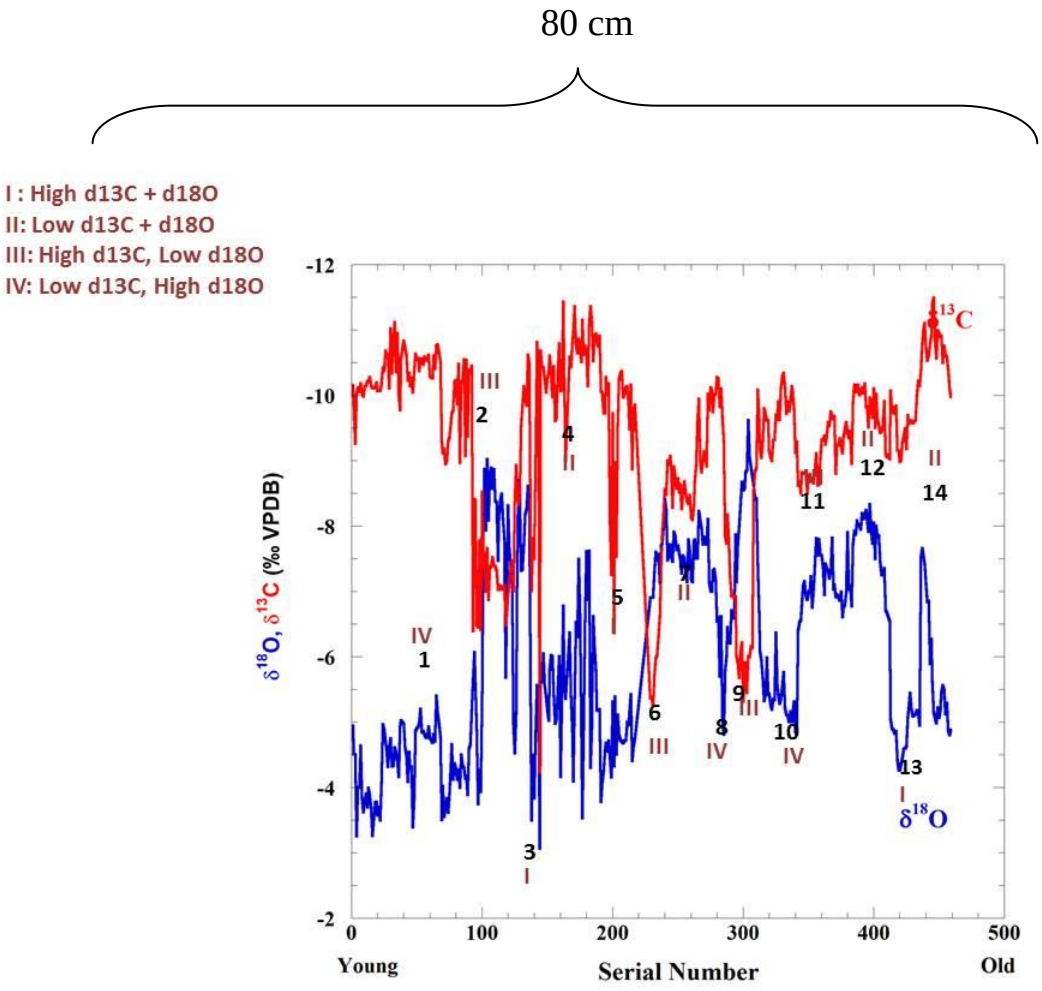

Figure 11: $\delta^{18}Oc$ and $\delta^{13}C$ profiles of TM-2 section vs serial number of the isotopic analyses points, the black number represent 14 events characterized by 4 different trends of $\delta^{18}Oc$ and $\delta^{13}C$

This isotopic profile is based on 459 isotopic analyses points drilled ~0.5 – 1.0 mm apart. The profile is characterized by significant fluctuations of both $\delta^{18}O_c$ and $\delta^{13}C$ values. Throughout the entire studied section, $\delta^{18}O_c$ values vary between -9.6‰ and -3‰. The $\delta^{13}C$ values range between -11.5‰ and -4.3‰ with maximum fluctuation between adjacent isotopic analyses points 143-144 of ~ 6 ‰.

The isotopic record was divided to 14 events characterized by 4 different combinations of $\delta^{18}O_c$ and $\delta^{13}C$ trends:

I. High $\delta^{13}C$ and high $\delta^{18}O_c$ (events 13, 5, 3)

II. Low $\delta^{13}C$ and low $\delta^{18}O_c$ (events 14, 12, 7, 4)

III. High $\delta^{13}C$ and low $\delta^{18}O_c$ (events 11, 9, 6, 2)

IV. Low $\delta^{13}C$ and high $\delta^{18}O_c$ (events 10, 8, 1)

4.3 Petrography and isotopic profile

This chapter presents a description of the calcite crystals of TM-2 (flowstone) cross-section, in order to define if growth was continuous and if there were major depositional changes during the formation of the flowstone. Special attention will be given to verify if changes in the crystal growth habits and size correspond to changes observed in the isotopic profile and therefore the numbers 1-14 represent the isotopes events described in section 4.2.

TM2-1B (event No. 1, Figure 12)

Two patterns are observed in the sample: (1) The oldest part, between isotopic analyses points 48-31 is characterized by very large (~ 10 mm) and transparent crystals with mosaic structure. Along this section, $\delta^{18}O$ values show moderated decreasing trend from -3.5‰ to -5‰. (2) The younger part of the section, between isotopic analyses points 31-23, is characterized mostly by small (1-2 mm) columnar crystals with parallel extinction**,** with dark laminae in between. Along this part, $\delta^{18}O$ values are characterized by fluctuations between -4‰ and -5‰. In both sections, the $\delta^{13}C$ values are relatively low, ranging between ~ -11‰ and -10‰. Although there are changes in the crystal habit, no sharp oscillations in the $\delta^{18}O$ and $\delta^{13}C$ are observed.

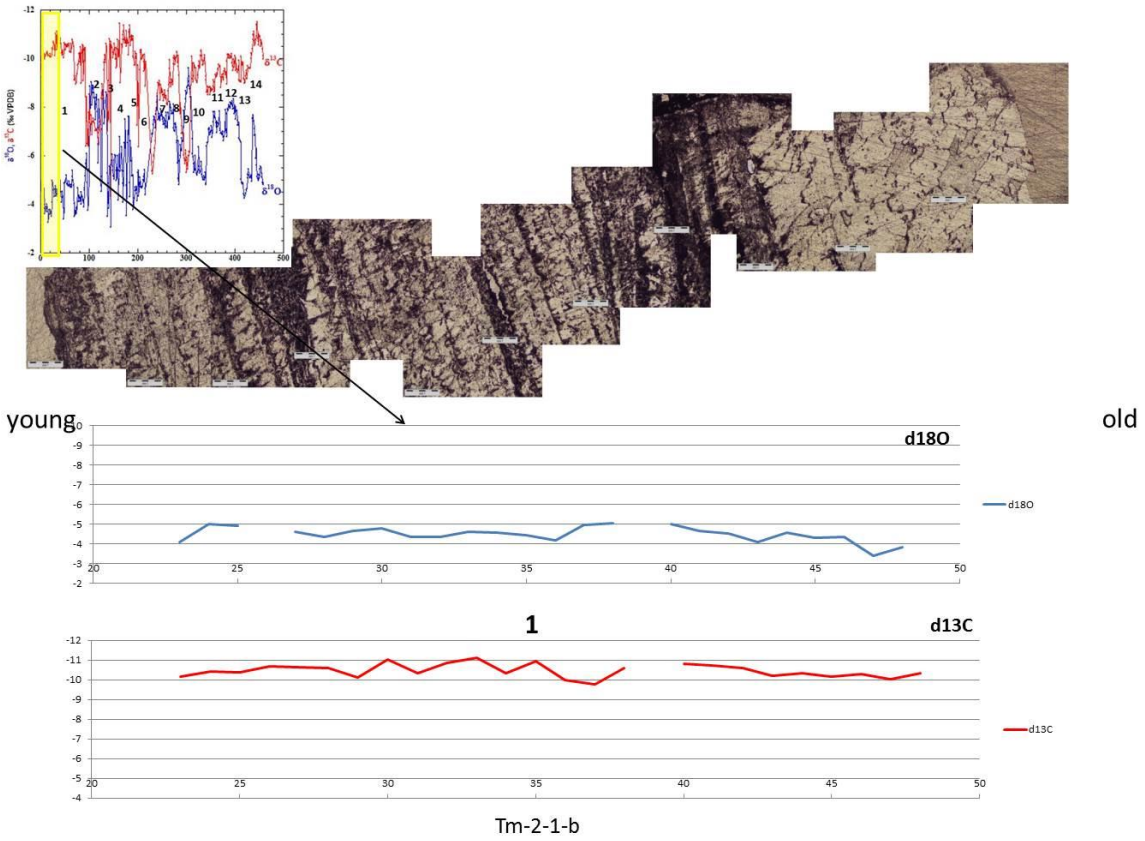

Figure 12: Comparison between petrography and isotopic record of TM-2-1-b covering the isotopic analyses points 23-48.

Tm2-1C (event No. 1, Figure 13)

In this section, the contact with the young cover that deposited on the quarry surface is observed. The older part of the section covers the isotopic analyses points 68-49. The oldest part (isotopic analyses points 68-61) is characterized by very long crystals (~10mm) oriented parallel to the contact with the young cover. The isotopic record is characterized by almost uniform $\delta^{18}O$ values (~-5‰) and low $\delta^{13}C$ (-10 to -11‰).

The younger part (between isotopic analyses points 60-49), show significant change in the petrography, characterized by smaller idiomorphic crystals, slightly rounded, oriented diagonally to the contact with young cover. The location of the rounded crystals between columnar crystals may indicate recrystallization. The entire isotopic profile is characterized by relatively stable $\delta^{18}O$ and $\delta^{13}C$ values, with very low amplitude. Between isotopic analyses points 56-68, the isotopic record is characterized by relatively high $\delta^{18}O$ values (-4.5 to -5.5‰) and low $\delta^{13}C$ values (-10 to -11‰).

In this sample, the significant variations in the petrography are not reflected in the isotopic composition.

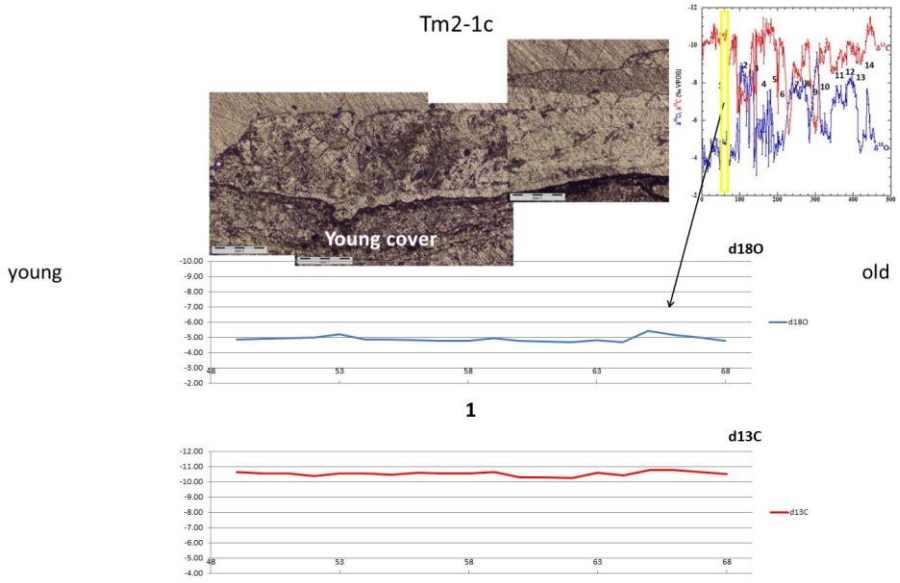

Figure 13: Comparison between petrography and isotopic record of TM-2-1-c, covering the isotopic analyses between points 50-68. The lower dark part is the young cover that deposited on the quarry surface.

Tm2-2-1 (event No. 1, Figure 14)

The petrography of the old part (isotopic analyses points 92-77) is characterized by 2 mm crystals with mosaic pattern. $\delta^{18}O$ values range between -4.5‰ and -4.0‰. At the old part, with significant fluctuations in the $\delta^{13}C$ from -10.5‰ to -9.0‰.

The young section is characterized by medium (up to 5mm) columnar crystals with preferred orientation. The $\delta^{18}O$ and $\delta^{13}C$ values increase from the older part to the younger part. Between isotopic analyses points 76-69 both $\delta^{18}O$ and $\delta^{13}C$ are higher, $\delta^{18}O$ values vary between -3.5‰ and -4.0‰, and $\delta^{13}C$ values are ~ -9.0‰.

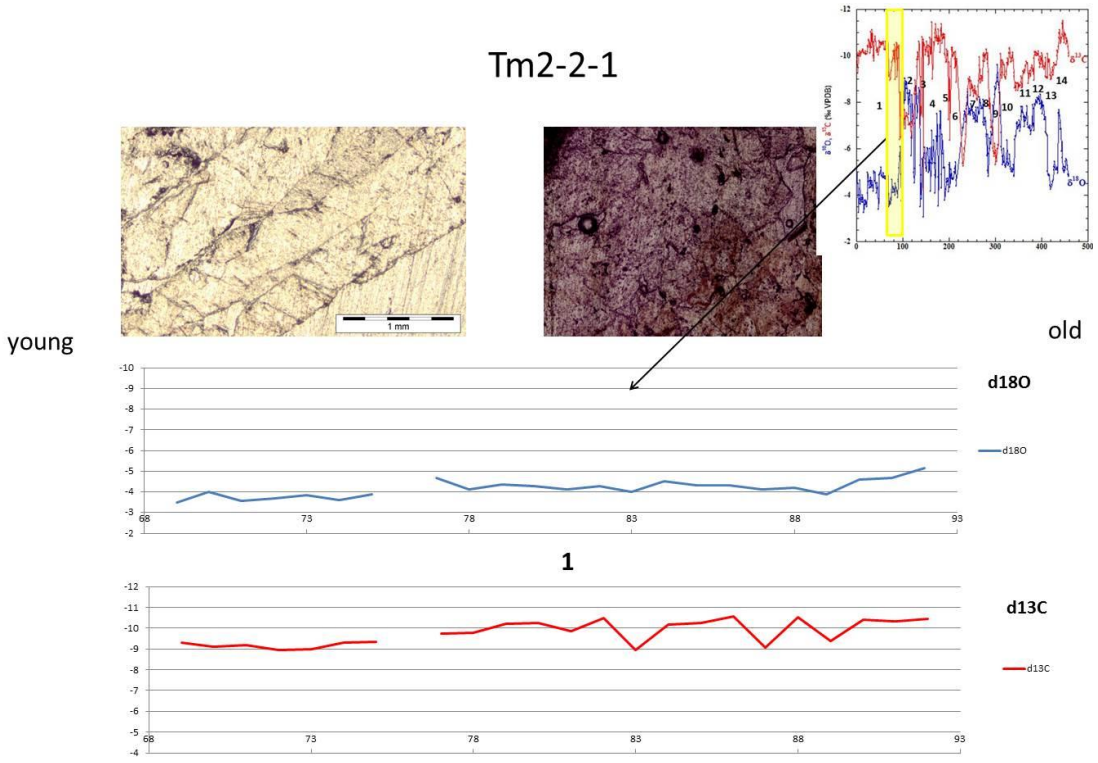

Figure 14: Comparison between petrography and isotopic record of TM-2-2-1 covering the isotopic analyses between points 92-69.

Tm2-2-2 (events No. 1&2, Figure 15)

The old part of the section (isotopic analyses points 117-104, event No. 2) is characterized by large (5 mm) crystals with mosaic pattern. The isotopic profile between isotopic analyses points 117-106 shows small fluctuations and is characterized by very low $\delta^{18}O$ values ranging between -7.5‰ and -9‰ coupled with high $\delta^{13}C$ values ranging between -7.0‰ and -7.5‰.

At ~ isotopic analyses points 104-101 the petrography is characterized by large columnar crystals (~4 mm in size). The amplitude changes in $\delta^{18}O$ values increases to ~1‰ from isotopic analyses point 106, and from isotopic analyses point 101 the $\delta^{18}O$ values increase, reaching a value of -4‰ until isotopic analyses point 97 (event No. 1). Overall, the $\delta^{18}O$ values increase significantly by ~5‰, from about -9‰ to -4‰. From isotopic analyses point 106 to 94, the amplitude of $\delta^{13}C$ fluctuations increase to 1‰-2‰, ranging from -8.5‰ to -6.5‰

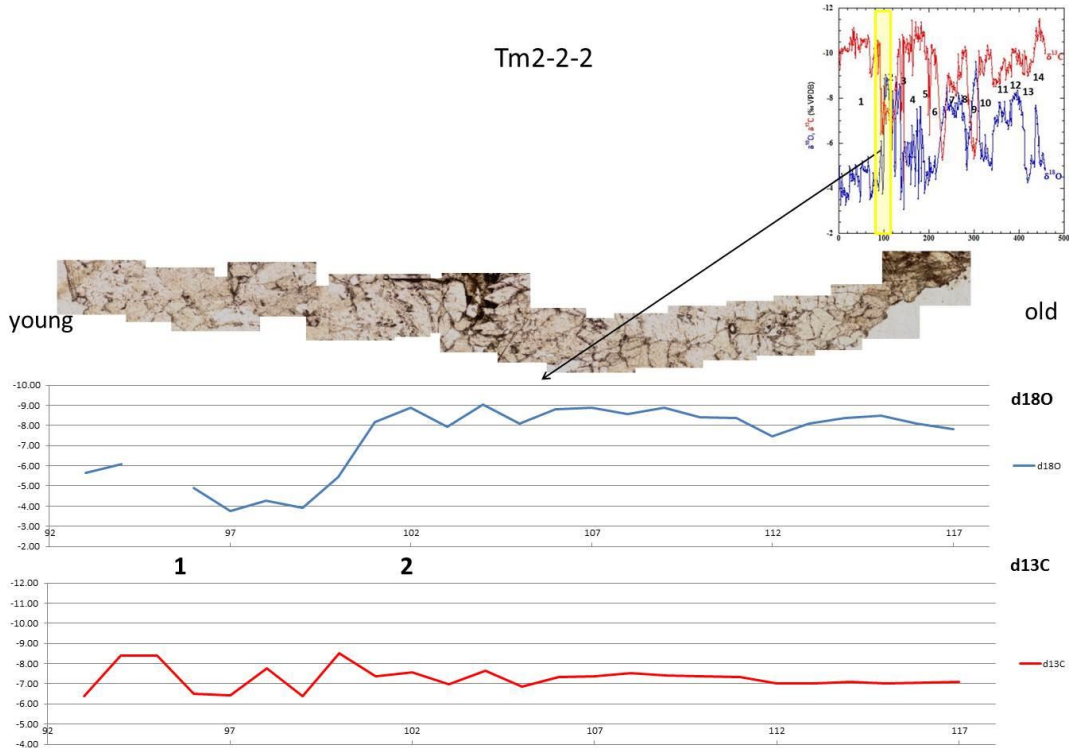

Figure 15: Comparison between petrography and isotopic record of TM-2-2-2 covering the isotopic analyses between points 93-117.

Tm2-2-3 (events No. 2&3, Figure 16)

The crystals at the older part (isotopic analyses points 136-130, event No. 3) are small (1-2 mm) with preferred orientation, forming laminar structure along the contact with the young cover. $\delta^{18}O$ values are very low, and moderately increase from -8.5‰ to -7.5‰.

The younger section (isotopic analyses points 130-118) is typified by long (10 mm) transparent crystals and the sample is characterized by dissolution voids.

Two $\delta^{18}O$ peaks (events No. 2&3) are observed in the young section, the first one is a high value of -4.5‰ at isotopic analyses point 125 and the second one a low value of -8.5‰ at isotopic analyses point 120, followed by an increasing trend to -5.5‰ at isotopic analyses point 118. $\delta^{13}C$ values show a continuous significant increasing trend throughout the entire sample, from -10.5‰ at the older part to -6.5‰ at the younger part.

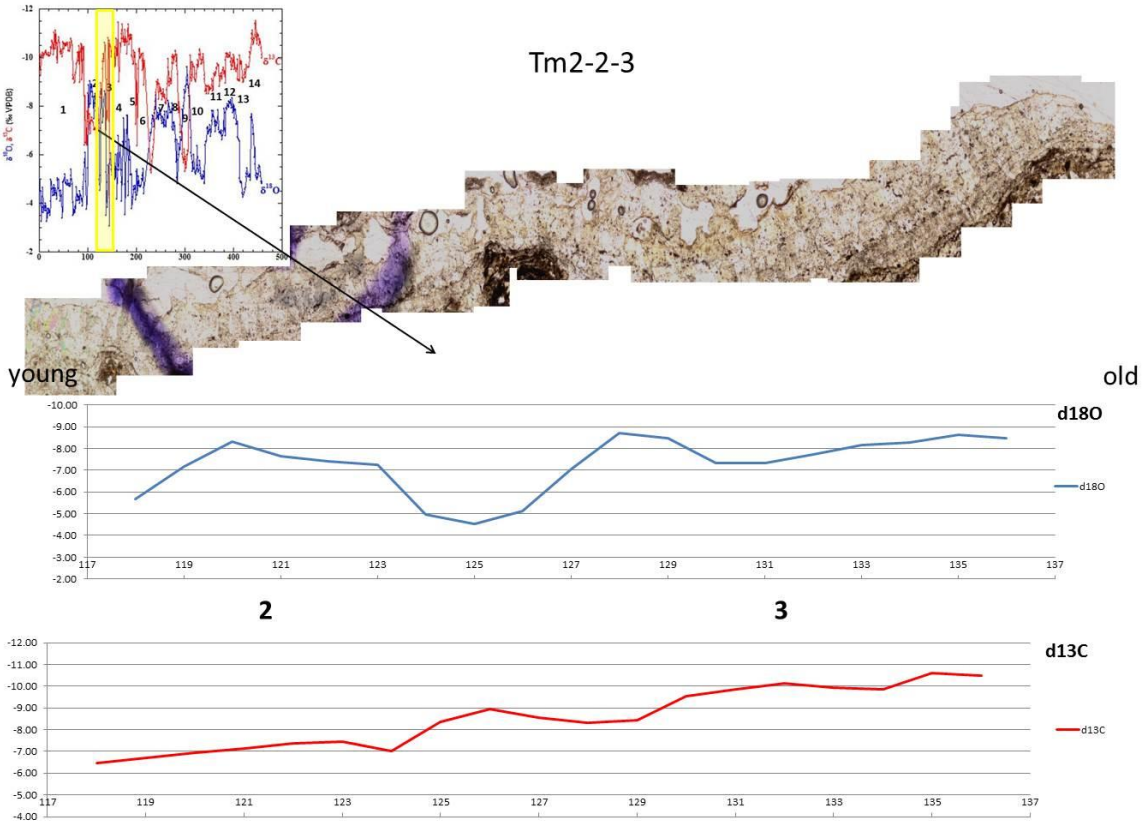

Figure 16: Comparison between petrography and isotopic record of TM-2-2-3 covering the isotopic analyses between points 136-118.

Tm2-3-ac (events No. 4&5, Figure 17)

The older part (isotopic analyses points 188-184, events No. 5) is characterized by large (5-7 mm) and clear crystals with preferred orientation.

The $\delta^{18}O$ profile of the entire sample is characterized by significant fluctuations with a high amplitude of ~ 3.5-4.0‰. From isotopic analyses points 188 to 183, there is decreasing trend from -5.0‰ to -6.5‰. A significant low $\delta^{18}O$ peak of -7.5‰ is observed at isotopic analyses points 180-178. This peak is also expressed by the petrography. The crystal size became smaller (0.5-2 mm) with interruptions of darks areas, most likely due to the presence of oxides and clays. At isotopic analyses points 174 and 172 there are two additional very low $\delta^{18}O$ peaks of -7.5‰ and -6.5‰ respectively.

Throughout the section, except the youngest part, $\delta^{13}C$ values are low, ranging between -10‰ and -11.5‰ with a constant increasing trend, and characterized by relatively much smaller fluctuations compared to the $\delta^{18}O$ values.

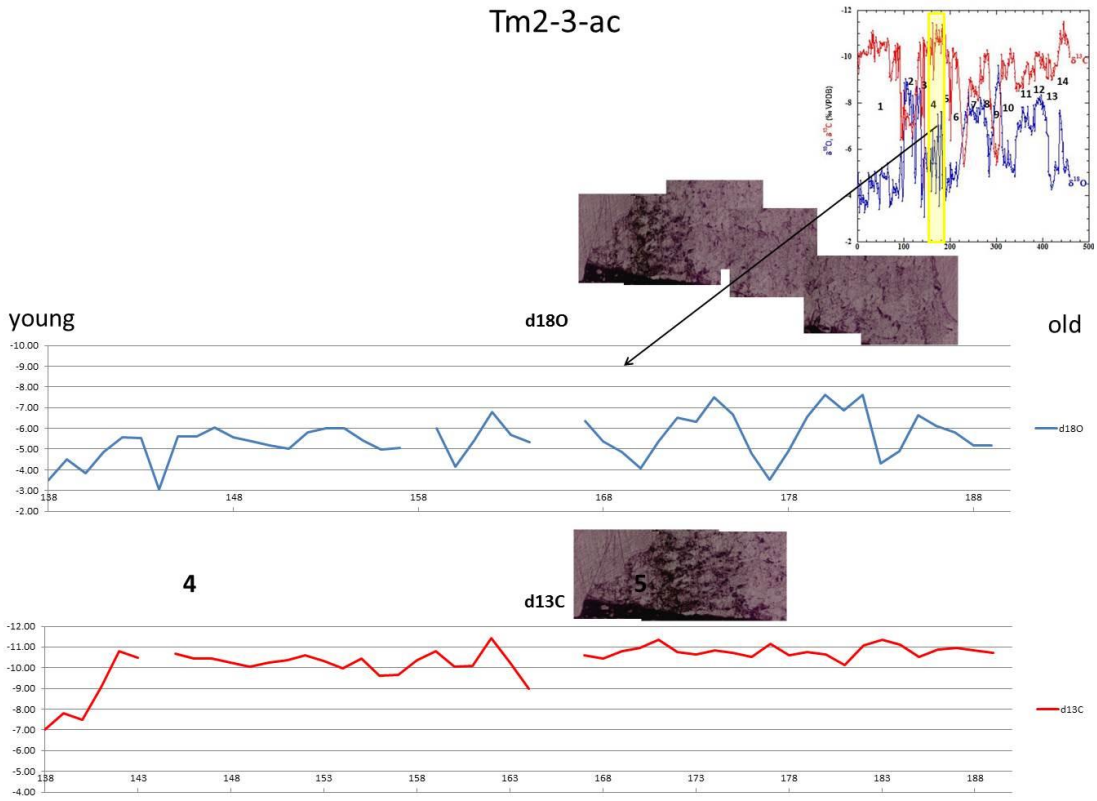

Figure 17: Comparison between petrography and isotopic record of TM-2-3-ac covering the isotopic analyses between points 188-138.

Tm-2-3-de (event No. 6, Figure 18)

The old part of the section (isotopic analyses points 216-205) is characterized by continuous growth of large and clear columnar crystals (5-20 mm). Isotopic composition is relatively stable and high: $\delta^{18}O$ values vary between -4.5 and -5.0‰, $\delta^{13}C$ between -9.5 and -10.5‰.

Around isotopic analyses point 205 (to isotopic analyses point 196), there is a change in the trends of the isotopic profiles, and both, $\delta^{18}O$ and $\delta^{13}C$ fluctuate in larger amplitude, in the order of 1‰ ($\delta^{18}O$) and 3‰ ($\delta^{13}C$). These significant variations in the isotopic profiles are also expressed by the petrography, which is characterized by few small crystals.

Between isotopic analyses points 198-191 the section is characterized by large crystals (10 mm) and relatively stable isotopic composition. $\delta^{18}O$ decreases from -3.8‰ to -4.7‰ and $\delta^{13}C$ form a plateau around -10‰.

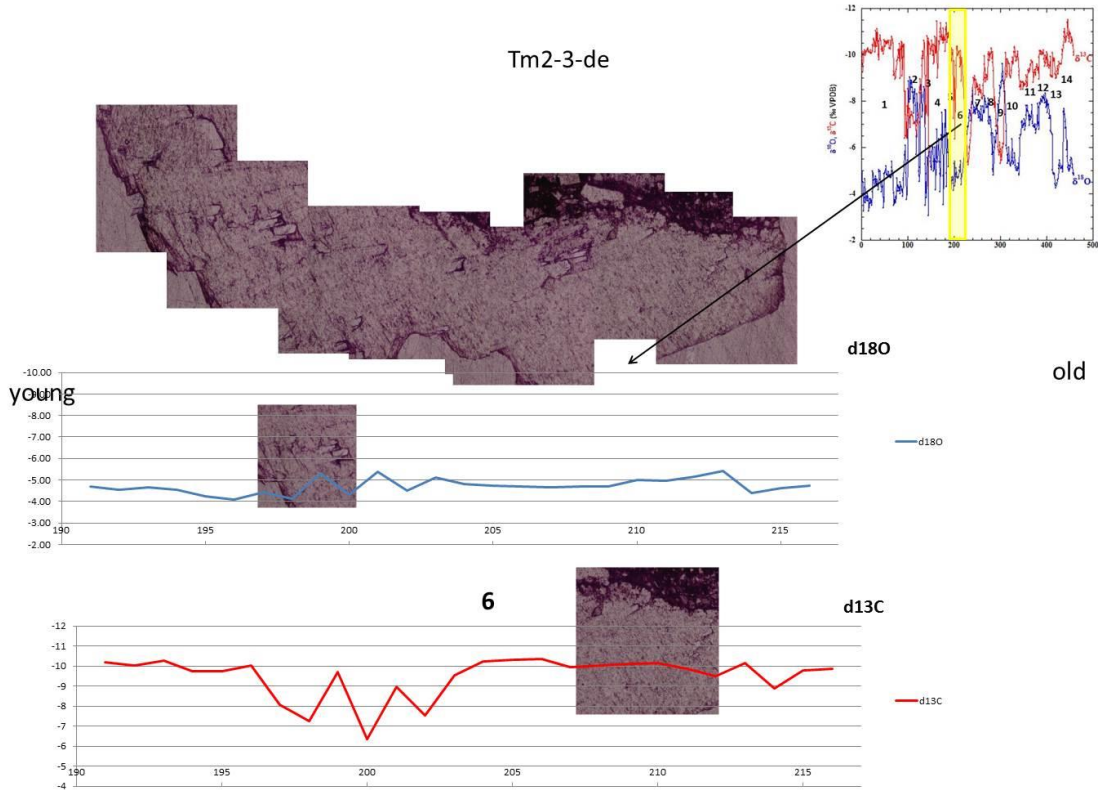

Figure 18: Comparison between petrography and isotopic record of TM-2-3-de covering the isotopic analyses between points 191-216.

TM2-4-1 (event No. 7,Figure 19)

The older part of the section (isotopic analyses points 270-247) is characterized by large and clear columnar crystals (5-8 mm) with preferred orientation, interrupted by an area of small crystals between isotopic analyses points 265-263. The isotopic profiles between isotopic analyses points 268-242 show low $\delta^{18}O$ values with small variations, $\delta^{18}O$ values fluctuating from -8 to -7‰. $\delta^{13}C$ values in this interval are relatively high fluctuating between -10 and -8‰.

The section between isotopic analyses points 246-237 is characterized by smaller crystals with no clear orientation.

The youngest part of the section (between isotopic analyses points 242-229), is characterized by growth of large and clear crystals (5-8 mm) while both isotopic profiles show increasing trends, $\delta^{18}O_c$ by a moderate range of ~ 1‰ (from -8 to -7‰), $\delta^{13}C$ by a very sharp increase of ~ 3‰ (from -8.5 to -5.5‰).

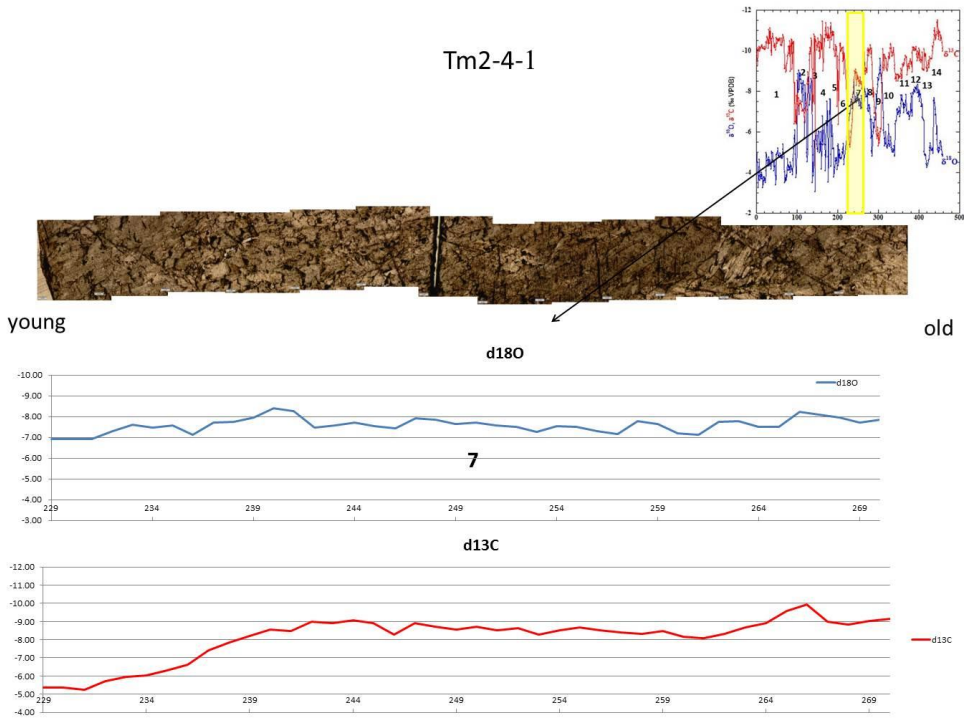

Figure 19: Comparison between petrography and isotopic record of TM-2-4-1 covering the isotopic analyses between points 229-270.

TM2-4-2 (events No. 9 & 8, Figure 20)

The older part of the section (isotopic analyses points 315-278, event No. 9) is characterized by continuous growth of large and clear columnar crystals (5 to >20 mm). From isotopic analyses point 315, there is a very sharp decrease in the $\delta^{18}O$ values (of ~ 3.5‰; from ~-6‰ to -9.5‰) reaching a very low $\delta^{18}O$ peak of -9.5‰. This very low $\delta^{18}O$ peak is coupled with high $\delta^{13}C$ peak of similar order of magnitude (~4.5‰; from ~-10‰ to -5.5‰) reaching a value of -5.5‰. The younger part of the section (isotopic analyses points 277-268, event No. 8) is characterized by smaller crystals (1 mm and less). It is characterized by an opposite isotopic trend, high $\delta^{18}O$ values (increasing to -4.8‰) coupled with low $\delta^{13}C$ (decreasing to -9.3‰). The different isotopic trends are also expressed by the petrographic pattern: there is a significant change from isotopic analyses points 285 to the younger section, and the continuous large and clear columnar crystals are replaced by much smaller crystals forming a laminar structure. Very thin white laminae expressed as dark thin layer maybe mark hiatuse (see arrow in Figure 20).

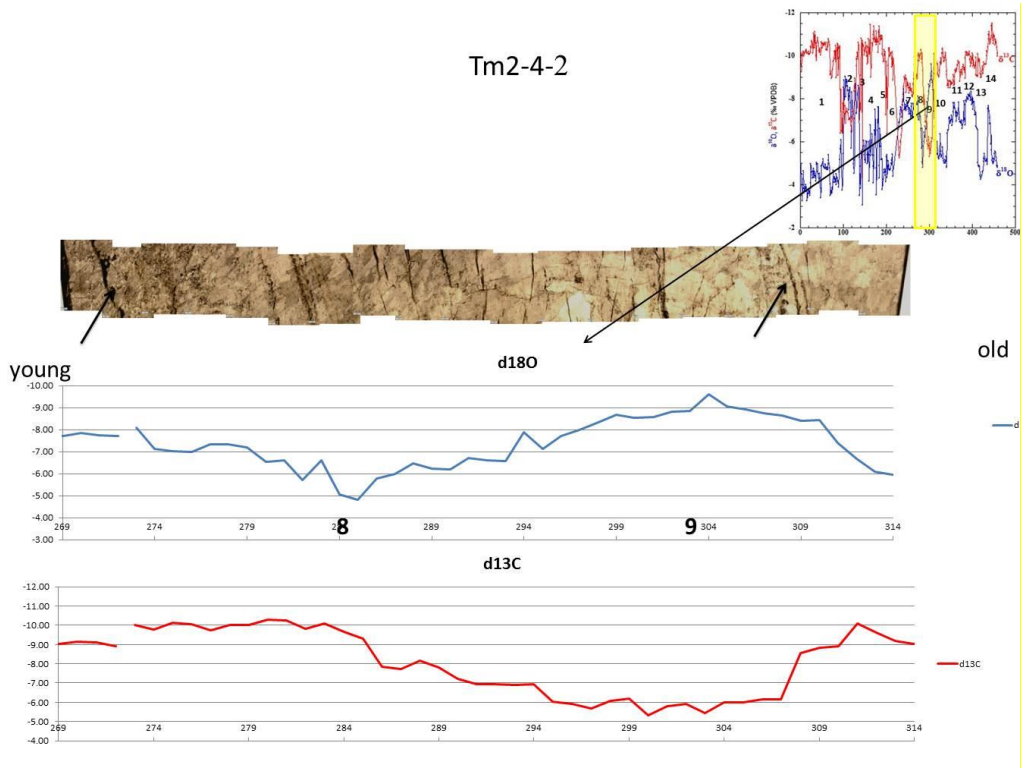

Figure 20: Comparison between petrography and isotopic record of TM-2-4-2 (covering the isotopic analyses between points 269-314.

TM2-4-3 (events No. 10, Figure 21)

The section (isotopic analyses points 341-310; event No. 10) is characterized by continuous growth of large and clear columnar crystals (5-10 mm). Around isotopic analyses points 335, 324 and 319 there are areas with small crystals (around 0.5 mm), similar to the pattern observed for event No. 8.

The entire section is characterized by relatively high $\delta^{18}O$ values varying from -5 to -6‰, coupled with low $\delta^{13}C$ values (–9‰ to –10.3‰). At the young edge (isotopic analyses points 316-310) there is a significant decreasing trend at $\delta^{18}O$ values from -5.5‰ to -8.5‰, with no significant change in the $\delta^{13}C$ values.

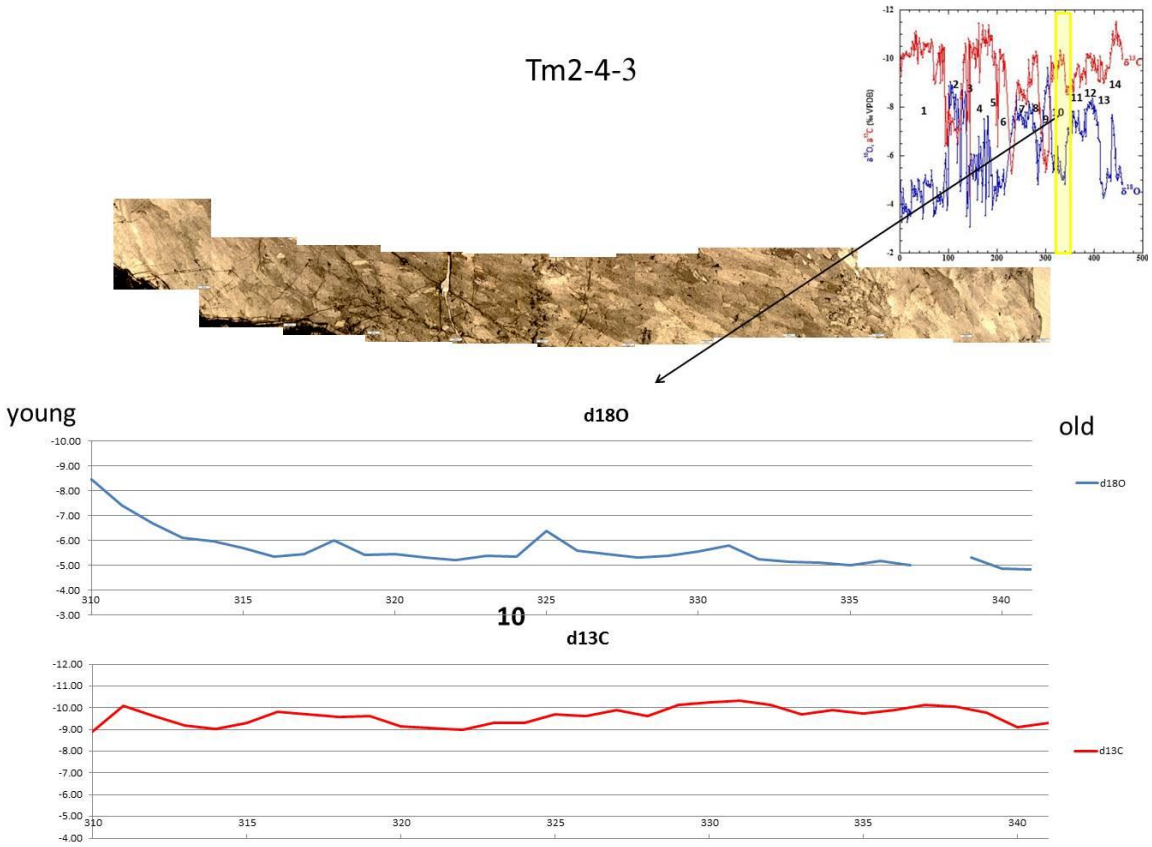

Figure 21: Comparison between petrography and isotopic record of TM-2-4-3 covering the isotopic analyses between points 310-340.

TM2-5 (event No. 11, Figure 22)

This section covers the isotopic analyses points 341-370.

Between analyses 368 to 356 there are large (8-10 mm) crystals interrupted by thin lamina and small (0.5 mm) crystals.

Throughout the entire section, $\delta^{18}O$ values are relatively low, varying between -7.8 and -6.8‰. $\delta^{13}C$ values show a continuous gentle increasing trend from -9.7‰ (isotopic analyses point 370) to -8.6‰ (isotopic analyses point 349). Around the isotopic analyses point 357, the $\delta^{18}O$ profile shows a low peak of -7.8‰ followed by an increasing trend toward isotopic analyses point 342. This part of the sample is characterized by large (8-10 mm) and homogeneous columnar crystals with preferred orientation.

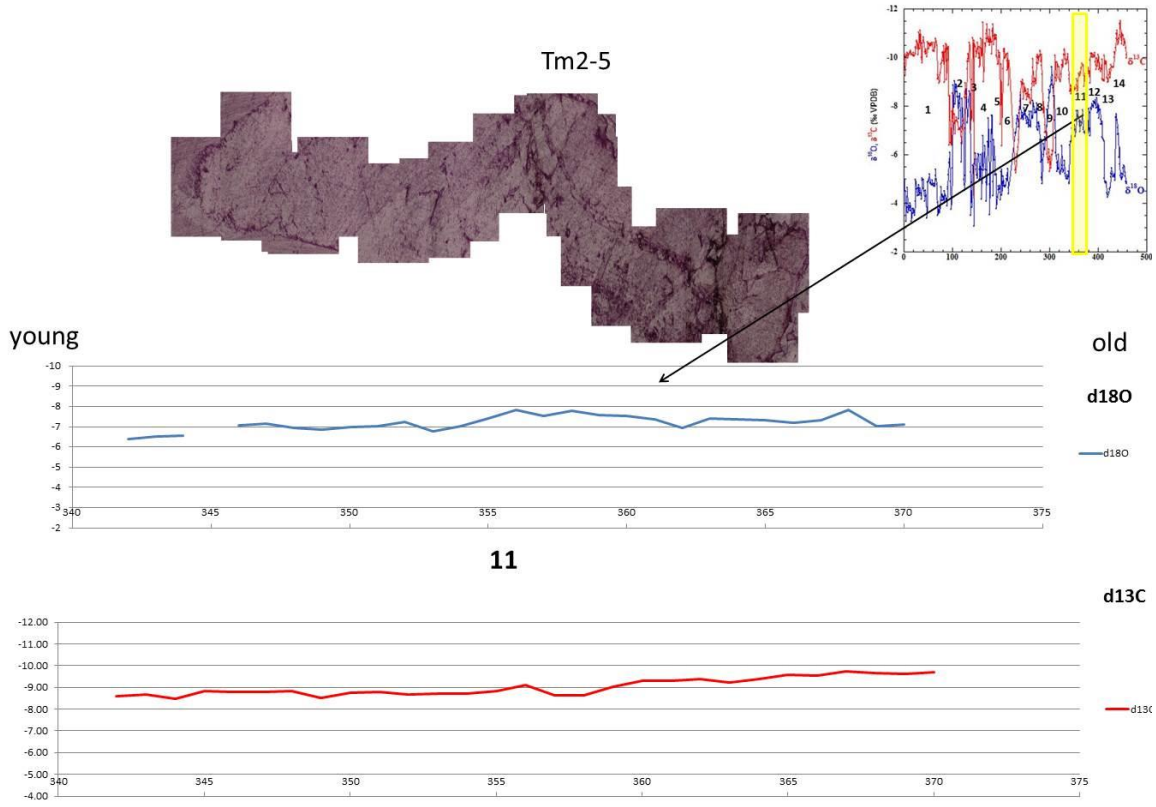

Figure 22: Comparison between petrography and isotopic record of TM-2-5 covering the isotopic analyses between points 341-370.

TM2-6 (event No. 12, Figure 23)

The petrography covers the isotopic analyses points 405-379. The older part is characterized by crystals with a mosaic structure; the crystals size is about 5 mm smaller. Between isotopic analyses points 412-395 there is a decreasing trend in both, $\delta^{18}O$ (from -6.5‰ to -8.2‰) and $\delta^{13}C$ (~ -9.0 to -10.0‰).

The younger part of the sample, between isotopic analyses points 395-384, is characterized by columnar crystals (5-20 mm) with parallel extinction. This section is characterized by relatively constant very low $\delta^{18}O$ values (-8.5‰ to -8.0‰) and $\delta^{13}C$ values (-10.2‰ to -9.8‰).

The youngest section of the sample (isotopic analyses points 384-379) is characterized by crystals with a mosaic structure. Both $\delta^{18}O$ and $\delta^{13}C$ are higher (-7.0 to -6.5‰ and -9.5 to -9.0‰ respectively)

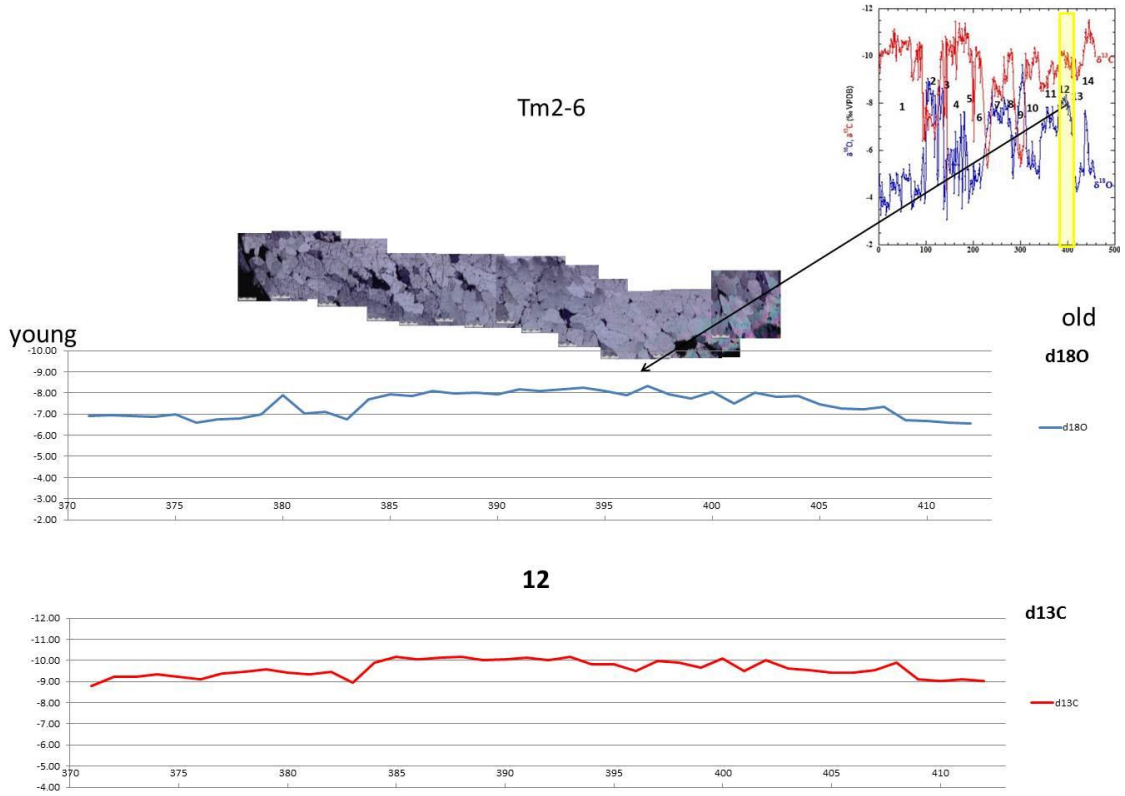

Figure 23: Comparison between petrography and isotopic record of TM-2-6 covering the isotopic analyses between points 405-379.

4.4 Isotopic composition of 'Bahat' archaeological artifacts

Figure 24 presents the $\delta^{13}C$ vs. $\delta^{18}O_c$ values of TM-2 section, and 'Bahat' archaeological artifacts from several archeological sites: Har Habait, Herodion, Caesarea, Tel Yarmuth, Kotel, Umm el Umdan,, N. Natuf and Herodian bathtub from Cypros fortress (Figure 25), and of archaeological artifacts from Egypt calcite alabaster. A flowstone sample from Abud Cave flowstone quarry was also measured for comparison.

The plot shows that $\delta^{18}O$ values from TM-2 section range between -9.6‰ and -3‰ and $\delta^{13}C$ values range from ~ -9‰ to -4‰. The isotopic composition of archaeological artifacts from Herodion, Kotel, Umm el Umdan, Abud Cave and N. Natuf fall in this range, whereas most artifacts from Egypt have lower $\delta^{18}O$ values ranging between -7‰ and -12‰ and higher $\delta^{13}C$ values ranging between ~ -5.0‰ and -8.5‰. Out of the five artifacts from Egypt, two samples cover the margins of TM-2 section.

The archaeological artifacts from Har Habait, Caesarea and Tel Yarmuth have very high $\delta^{13}C$ values (~ -1‰ to 4‰), and Herodian bathtub is characterized by lowest $\delta^{13}C$ values (~ -14‰).

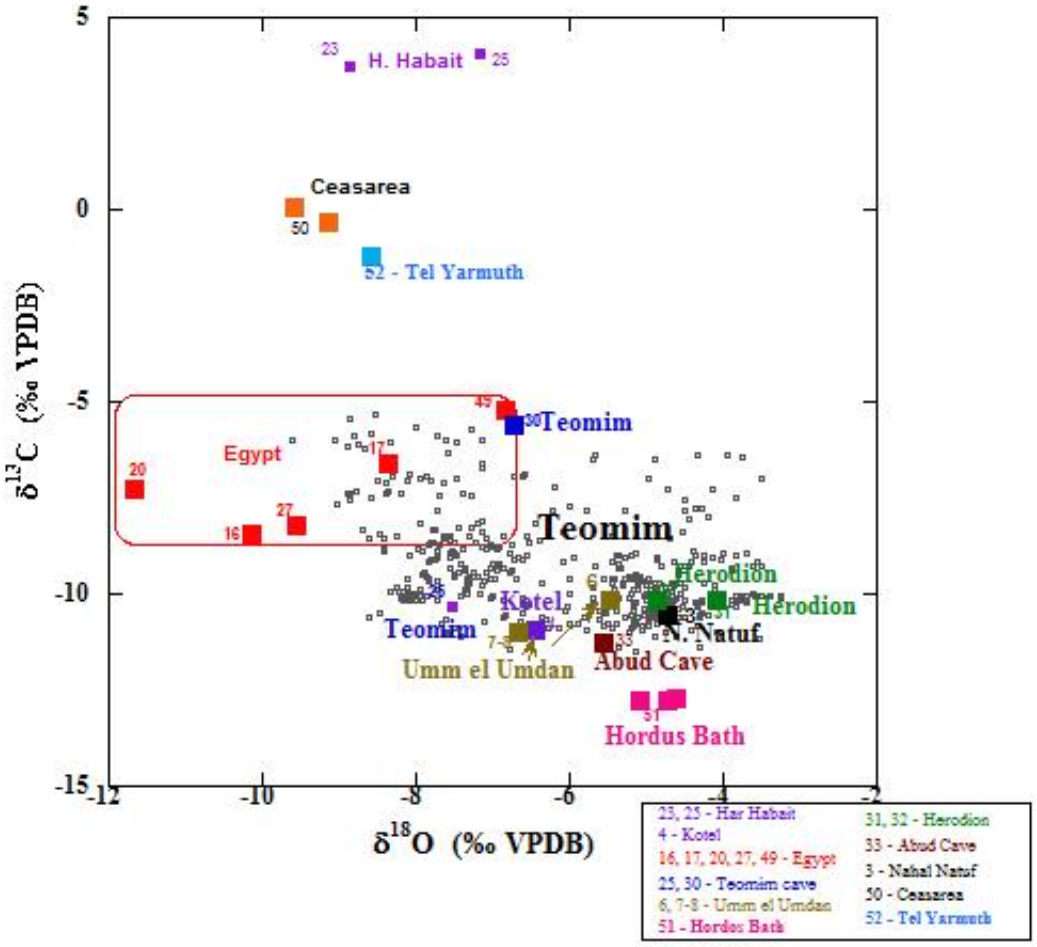

Figure 24: $\delta^{13}C$ plotted against $\delta^{18}O_c$ values of TM-2 section, and from 'Bahat' artifacts from various sources (see text and appendix 1 for details).

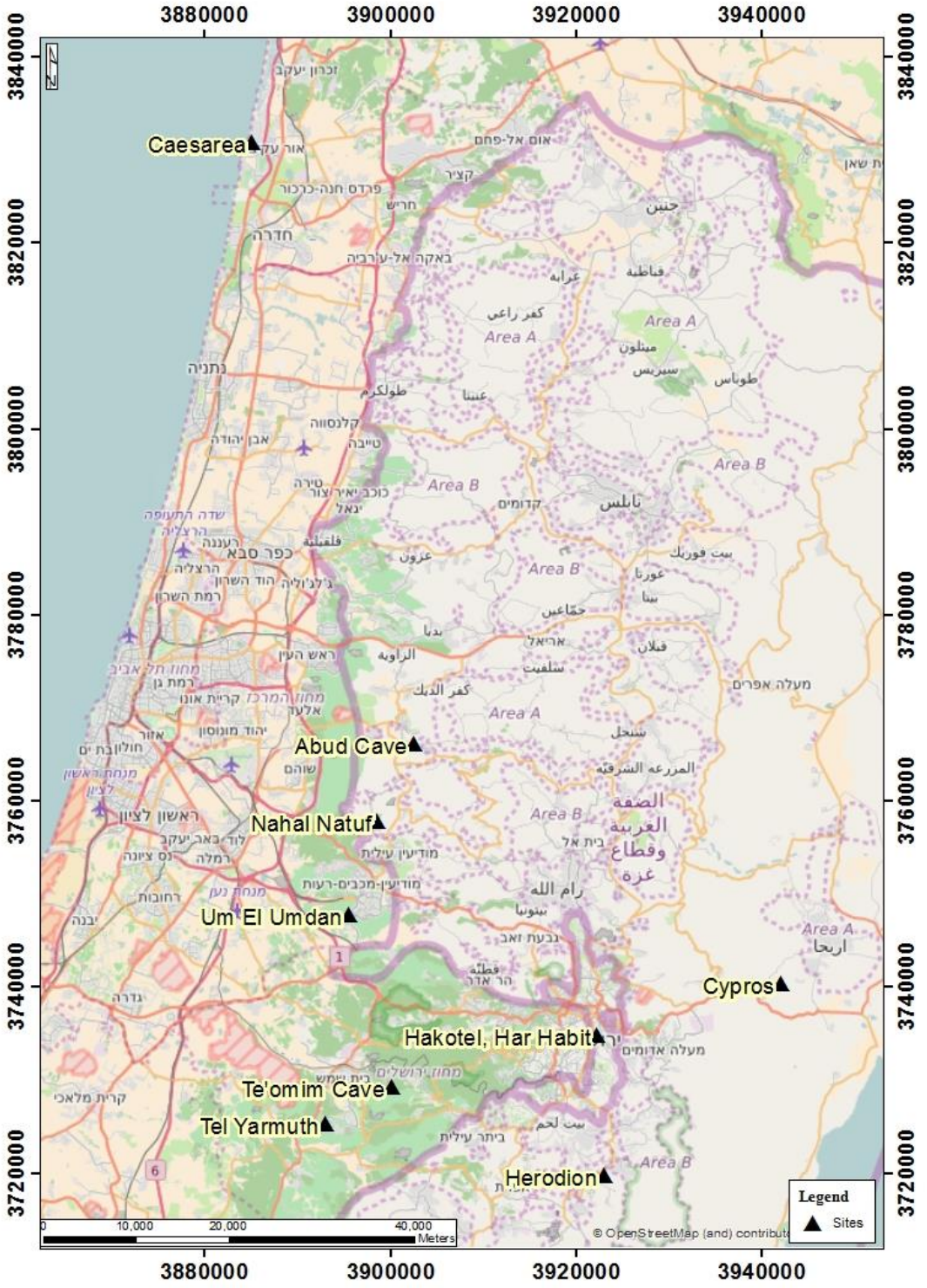

Figure 25: location map of the archeological sites**.**

5 Discussion

5.1 Dating

The dating of the section TM-2 was carried out using three different methods as described above in the methods (3.2) and the results (4.1) chapters. The methods include U/Th dating of the younger (upper) part, magneto-stratigraphy and U/Pb of the older part.
Top 10 cm of the flowstone grew between 773-53 ka and the mean growth rate is ~ 0.015 cm/ka.
The U/Pb dating (the 2 lower ages marked in blue in Figure 27) gave two similar ages of 1310 ±60 ka and 1350 ±120 ka, with ~40 cm of flowstone in between these dating points, suggesting very fast mean growth rates of 5.5-10 cm/ka.
The magneto-stratigraphic chronology gave five reversal ages from top to bottom: 773ka, 1001ka, 1069ka, 1189ka and 1221ka (marked in black in Figure 27).
The assumptions made for wiggle matching are as follows:
Using all the measured ages, TM-2 grew between 1350-60ka. The youngest part, the top 10 cm, grew very slow between 773-60ka, and provide a low resolution profile. The older 70 cm of the section, grew between ~1350ka and 773ka. The average growth rate is about 8cm/ka. At this time interval, 13 significant climate events were identified as described above. Out of the 13 events, 4 events (2, 6, 9 and 11) are characterized by low $\delta^{18}O_c$ and high $\delta^{13}C$ peaks, that usually identify sapropel events (Bar-Matthews et al., 2000; 2003; Frumkin et al., 1999). Event 2 at ~ 770 ka can match sapropel 17, event 6 at ~ 950 ka can match sapropel 18, event 9 at ~1100 ka can match sapropel 26, and event 11 at ~ 1170 ka can match sapropel 28. Using these dated "anchors", allows us to locate the older 70 cm of TM-2 section in the time interval of 1350-773 ka. Based on the determined time range, we can wiggle-match the significant isotopic events of TM-2 $\delta^{18}O_c$ profile with a global isotopic profile in this time interval.
For the wiggle-matching we correlated TM-2 low $\delta^{18}O_c$ peaks with the most significant low $\delta^{18}O_c$ peaks of LR04 benthic $\delta^{18}O_c$ stack (Lisiecki & Raymo 2005; Fig. 27). Lisiecki & Raymo (2005) published a 5.3-Ma stack (the ''LR04'' stack) of benthic $\delta^{18}O_c$ records

from 57 globally distributed sites aligned by an automated graphic correlation algorithm. LR04 age model for the Pliocene-Pleistocene is derived from tuning the $\delta^{18}O_c$ stack to a simple ice model based on 21 June insolation at 65N. The stack is plotted using the LR04 age model with MIS labels for the early Pleistocene.

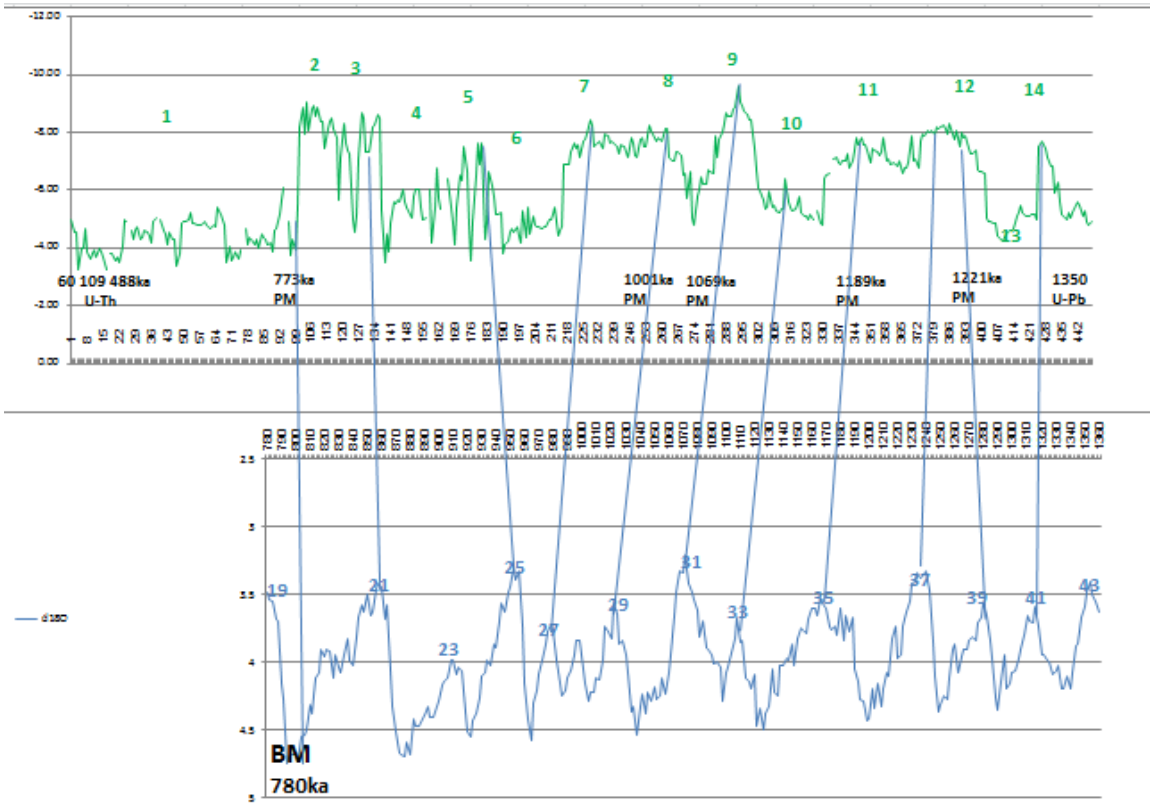

Figure 26: Wiggle matching between TM-2 $\delta^{18}O_c$ profile (green, upper graph) and the LR04 benthic $\delta^{18}O_c$stack (blue, lower graph; Lisiecki and Raymo, 2005). The black numbers are the age anchors (U-Th, PM-Paleomagnetism, U-Pb), the green numbers at the top diagram are the 14 isotopic events identified in TM-2 $\delta^{18}O_c$ profile and the blue numbers at the bottom diagram are marine isotopes stages (MIS).

Following the ages determined by U-Th, paleomagnetism, U-Pb, sapropels and the wiggle matching between TM-2 $\delta^{18}O_c$ profile and the benthic $\delta^{18}O_c$ stack, the measured and wiggle-matched ages are presented in Table 1. The composite $\delta^{18}O_c$ and $\delta^{13}C$ isotopic profiles of TM-2 plotted against the entire age interval (0 to 1400 ka) are shown in Figure 28a, and the high-resolution profile from 750 ka to 1400 ka is shown in Figure 28b.

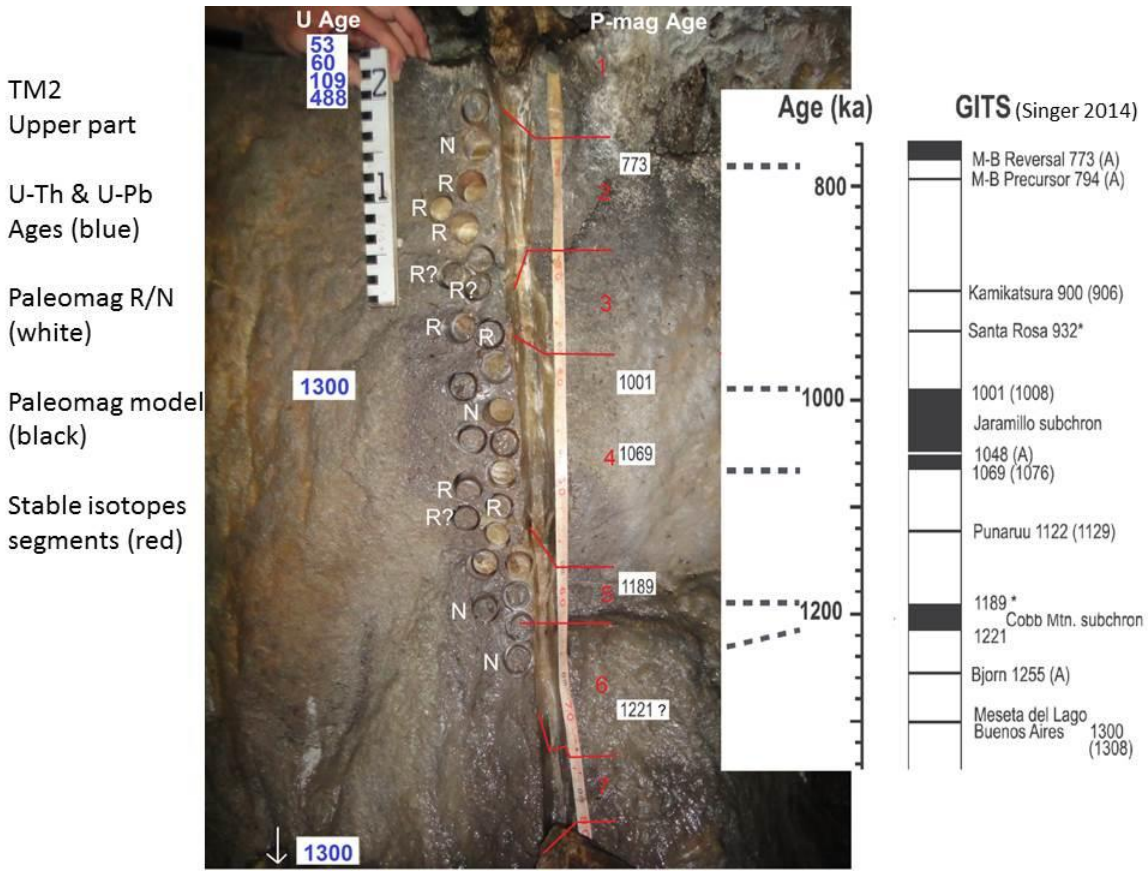

Figure 27: Dating results of TM-2 section: Ages from U/Th and U/Pb in ka are marked in blue, and magneto-stratigraphic results, R-reversal in black and N- normal in white. Magneto-stratigraphic time scale is according to Singer (2014) and marked in black on the right. The suggested correlation with magneto-stratigraphic results is indicated by dashed lines.

This method of determining ages by comparing isotope profiles by wiggle-matching them to a well-dated record, is well known in deep sea cores (e.g. Martinson et al., 1987; Imbrie et al., 1993; Hoek and Bohncke, 2001). Oxygen-isotope wiggle-matching provides a basis for time-parallel synchronizing between ice-core, terrestrial, and marine records (Hoek and Bohncke, 2001). The wiggle-matching dating technique used here is applicable in regions where climatic oscillations produced isotopic variations that can be recognized in the isotopic record (Kagan et al., 2005).

Table 1: ages determined by U-Th, paleomagnetism, U-Pb and the wiggle matching between TM-2 $\delta^{18}O_c$ and the benthic LRO4 $\delta^{18}O_c$ stack.

TM-2 Ser. No. *	Age ka	U-Th (ka)	PM (ka) **	U-Pb (ka)	Sapropel No.	MIS age (ka)	MIS Event	TM-2 Event No.	Time interval between TM-2 Events
1	60	60±0.8						1	
5	109	109±1.3						1	
15	488	488±87						1	
100	773		773		17			2	
136	860					860	21	3	87
182	950					950	25	5	90
233	950				18			6	
240	978					978	27	7	28
250	992		1001						
274	1024					1024	29	8	46
276	1027		1069						
304	1072				26	1072	31	9	48
325	1108					1108	33	10	36
344	1144		1189						
357	1168				28	1168	35	11	60
386	1240					1240	37		
396	1273		1221 ?						
398	1280					1280	39	12	112
420	1300					1300	41		
437	1316					1316		14	36
459	1350			1350±(60-120)					

*Isotopic analysis points

** Paleomagntism

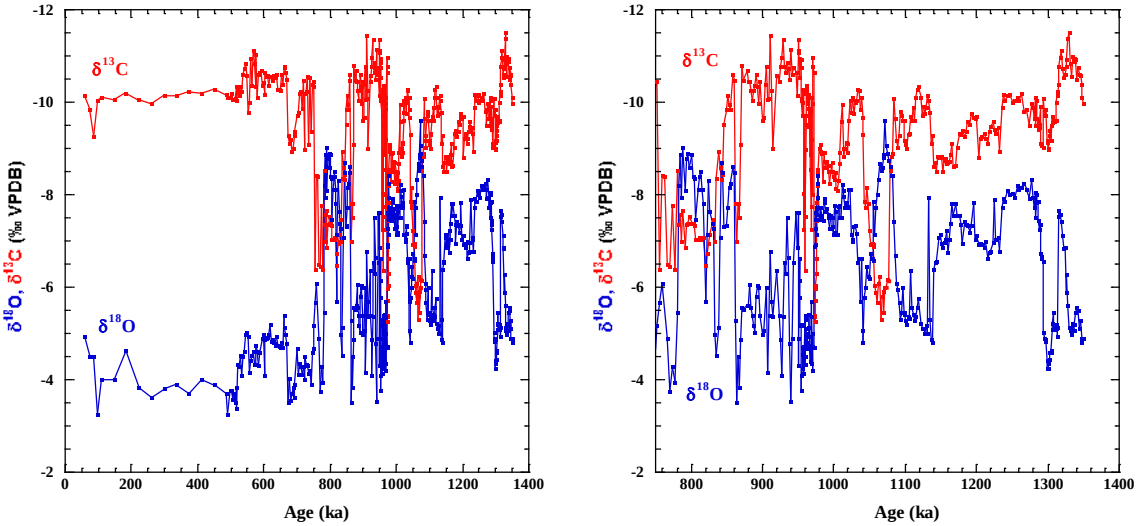

Figure 28: $\delta^{18}O_c$ and $\delta^{13}C$ isotopic profiles of TM-2 plotted against age, (A). 1350-0 ka, (B). 1350-750ka.

The average time interval between the peaks is about 40ka. This cyclicity matches the 41ka obliquity cycles that occur until the beginning of the MPT. The transition between peaks 2 to peak 1, that corresponds to the paleomagnetism Brunhes–Matuyama reversal at 773ka may represent the MPT in the TM-2 section. Differences observed between the TM-2 $\delta^{18}O_c$ record and the global record may reflect local climate conditions, which are further discussed below.

The isotopic record of TM-2 is indicative of a long period of flowstone growth since almost 1350ka. This record provides the longest terrestrial paleoclimatic record at the Mediterranean region. Several breaks in deposition (hiatus) were rarely identified within the Bruhnes paleomagnetic epoch, and the older flowstone deposition seems to be continuous, indicating that the drip and flow was partly diverted from TM-2 site during the mid-Pleistocene.

5.2 Isotopic profile characteristic features

As mentioned above, for comfortable description, the record was divided to 14 isotopic events (event 14 is the oldest and event 1 is the youngest, Figure 11).

As described in section 1.5.2, variations in the $\delta^{13}C$ values of calcite speleothems mainly reflect changes of the vegetation type in the vicinity of the cave, while other factors controlling the $\delta^{13}C$ values are presence or absence of soil cover, intensity of carbonate host-rock dissolution and water–rock interactions in the unsaturated zone.

The $\delta^{18}O_c$ values of speleothems depend on the temperature in the cave and the $\delta^{18}O_w$ of the cave water, which is closely related to the isotopic composition of the rainwater. Low $\delta^{18}O_c$ values are typical for interglacial periods. The low $\delta^{18}O_c$ values of TM-2 range between -7.5‰ and -9.5‰. These values are low in comparison to the interglacial low $\delta^{18}O_c$ values of Soreq cave at the last 250ka that reach a minimum value of about -8‰ (Figure 29). The high $\delta^{18}O_c$ glacial values of TM-2 are around -4‰, and are also low in comparison to Soreq values which are around -2 to -3‰. The $\delta^{13}C$ values of TM-2 section range between -5‰ and -12‰ while the values of Soreq profile range mainly between -8‰ and -13‰ (Figure 29).

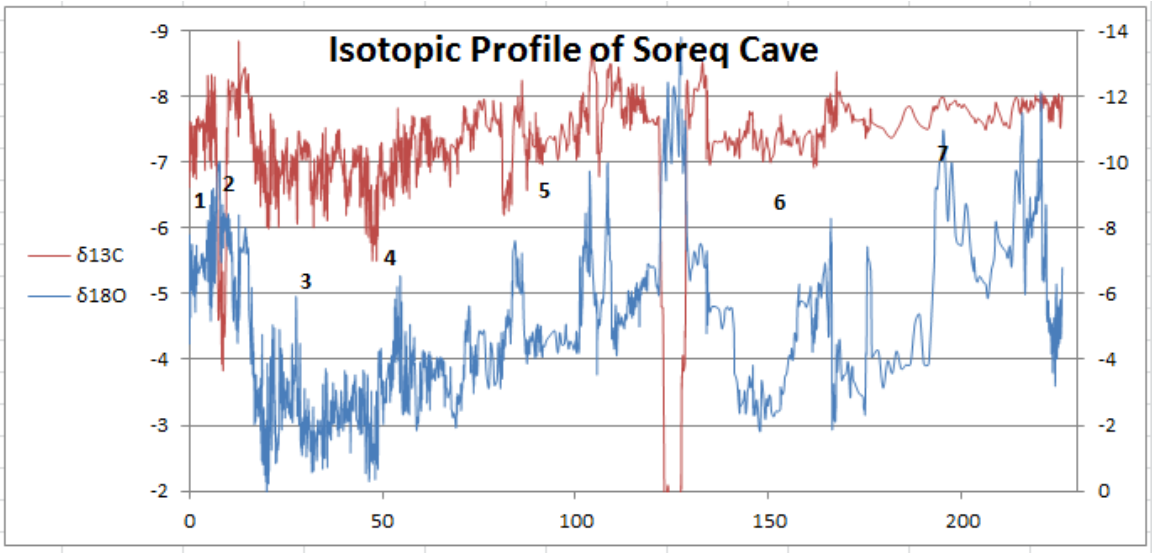

Figure 29: $\delta^{18}O$ and $\delta^{13}C$ isotopic profiles of Soreq Cave plotted against age, the black numbers are MIS events (Bar-Matthews et al., 2003; Bar-Matthews 2014).

The differences between the $\delta^{18}O_c$ and $\delta^{13}C$ values of TM-2 section at the mid Pleistocene and the values of Soreq cave at the last 230ka may indicate different climatic systems. This difference is also reflected at 40ka cyclicity observed in the TM-2 section that matches the 41ka obliquity cycles that occur until the beginning of the MPT, compared with the 100ka cyclicity at the late Pleistocene.

There are four events observed at the TM-2 isotopic profile which are characterized by low $\delta^{18}O_c$ values associated with high $\delta^{13}C$ values (events 11, 9, 6 and 2; Figure 11). High $\delta^{13}C$ values usually indicate dry conditions and relatively low biogenic activity and low vegetation root zone respiration rates (e.g., Quade et al., 1989a), and high ratio of C4 to the C3 biomass. Low $\delta^{18}O_c$ values usually do not match the high $\delta^{13}C$ values. The coupling between low value of the $\delta^{18}O_c$ and high $\delta^{13}C$ values of can be also interpreted as reflecting deluge events, where $\delta^{13}C$ values do not reflect the soil-CO_2 composition, due to high rate of water flushing to the cave, resulting in isotopic composition approaching the surrounding dolomite host rock (e.g., Bar-Matthews et al., 2000). Alternatively, high $\delta^{13}C$ values can be the outcome of unstable, dry and warm conditions, loss of vegetation, and erosion of the soil cover. This hydrologic regime is consistent with irregular high water flushing events: flash-floods are potentially more common under scarce vegetation cover. Such fluctuating dry-hot intervals could have enhanced forest fires, followed by rapid soil erosion; eventually leading to abrupt changes and high $\delta^{13}C$ values (Frumkin et al., 2000). These periods occur at 1168 ka, 1072 ka, 960 ka and 830 ka (peaks 11, 9, 6 and 2 respectively). Peaks 11 and 9 are correlated with sapropel events 35 and 31 respectively.

5.3 The relations between the petrography and the isotopic profile

As described above, combining the $\delta^{13}C$ and $\delta^{18}O$ trends, four categories have been observed. In some cases, these isotopic trends are associated with significant petrographic structures. In general, most of the flowstone section is characterized by large columnar crystals, leading for the typical 'Bahat' structure. Though in some cases similar petrographic features are found for different isotopic peaks from the same category, it is not always so, and isotopic peaks from the same category may be associated with different petrographic features.

(I) High $\delta^{13}C$ and high $\delta^{18}O$ (peaks 13, 5, 3)

Event 5 and 3 (Figure 18 and Figure 16 respectively) are characterized by small crystals interrupting large and massive calcite crystals structure. The combination of the isotopic composition of high $\delta^{13}C$ and high $\delta^{18}O$, and the petrography, small crystals indicate slow and inconsistent growth, most likely reflecting relatively dry conditions

(II) Low $\delta^{13}C$ and low $\delta^{18}O$ (events 14, 12, 7, 4)

Peaks 12 and 7 are characterized by large crystals, reaching up to 10-20 mm, in some places forming a mosaic structure (Figure 23 and Figure 19 respectively). The combination of the isotopic composition of low $\delta^{13}C$ and low $\delta^{18}O$, and the petrography, large, mostly not oriented crystals indicate continuous growth, most likely reflecting relatively wet conditions. Such wet conditions are not always reflected in the petrographic structure.

(III) High $\delta^{13}C$ and low $\delta^{18}O$ (peaks 11, 9, 6, 2)

Peaks 11 and 2 show similar petrography. Peak 11 is characterized by large (8-10 mm) and transparent homogenous columnar crystals with preferred orientation (Figure 22), and peak 2 is typified by long transparent crystals (~10 mm; Figure 16). Peaks 9 and 6 are also characterized by large and clear columnar crystals (5-8 mm) with preferred orientation, but interrupted by an area of small crystals (Figure 20 and Figure 18 respectively).

The combination of high $\delta^{13}C$ values coupled by low $\delta^{18}O$ values may indicate periods of relatively dry (high $\delta^{13}C$) and warm (low $\delta^{18}O$) conditions. However, as clearly seen in peaks 9 which is characterized by very sharp decrease in $\delta^{18}O$ values (from ~ -5 to -9‰) coupled with very sharp increase in $\delta^{13}C$ values (from ~ -10 to -5.5‰), these climatic conditions may reflect a sapropel event which is characterized by high hydrologic activity, resulting in very low $\delta^{18}O$ values. As explained by Bar-Matthews et al (2003), the high $\delta^{13}C$ values during the sapropel event may be due to deluge conditions, resulting in minimum reaction between the water and the soil CO_2. Alternatively, Frumkin et al. (2000) suggest that the high $\delta^{13}C$ during sapropel events

could be the outcome of unstable, dry and warm conditions, loss of vegetation, and erosion of the soil cover.

(IV) Low $\delta^{13}C$ and high $\delta^{18}O$ (peaks 10, 8, 1)

Peak 10 is characterized by medium-large and clear columnar crystals (5-10 mm) with preferred orientation, interrupted in places by an area of small crystals (Figure 21). Peak 8 is characterized by smaller crystals without preferred orientation. On the other hand, peak 1 is characterized by various petrographic features, including large tabular crystals, laminated medium-size crystals, and large crystals with mosaic structure.

The combination of low $\delta^{13}C$ and high $\delta^{18}O$ values may reflect wet (low $\delta^{13}C$ values) and cold (high $\delta^{18}O$ values) climatic conditions. The large and clear calcite crystals most likely reflect continuous and constant growth.

5.4 Isotopic composition of 'Bahat' archaeological artifacts

Figure 24 presents the $\delta^{13}C$ plotted against $\delta^{18}O$ values of TM-2 section, and of 'Bahat' archaeological artifacts from several archeological sites. The plot shows that $\delta^{18}O$ values from TM-2 section range between -9.6‰ and -3‰ and $\delta^{13}C$ values range from ~ -11.5‰ to -4‰. Archaeological artifacts from Har Habait are characterized by very high $\delta^{13}C$ values (+4.1‰ and +3.7‰), relatively to the values of the Te'omim cave, coupled with low $\delta^{18}O$ values of -8.9‰ and -7.2‰. These artifacts are not made of 'Bahat' but probably from marble. Archaeological artifacts from Caesarea and Tel Yarmuth are also characterized by relatively high $\delta^{13}C$ values (~0‰ and -1.2‰ respectively) coupled with low $\delta^{18}O$ values (~-9.3‰ and -8.6‰ respectively). These artifacts are also probably most likely not made of the 'Bahat' quarried at the Te'omim cave quarry.

Most measured archaeological artifacts from Egypt (samples 20, 16 and 27, see Figure 24) are characterized by significantly lower $\delta^{18}O$ values (ranging between -6.8‰ and -11.7‰) than Te'omim cave values, whereas $\delta^{13}C$ (range between -5.2‰ and -8.5‰), is similar to the higher $\delta^{13}C$ values measured for Te'omim Cave. Samples 17 and 49 have values that match the margins of the Te'omim Cave values, but to find the provenance of

these artifacts requires using other methods (e.g., trace elements, Sr isotopic composition).

$\delta^{18}O$ value of the sample taken from Herodian buthtub is in the middle of the range of Te'omim Cave samples (~ -5‰), while the $\delta^{13}C$ is ~-13‰, below the range of the values from the Te'omim cave, lower also than all other 'Bahat' samples measured in this study. Therefore, probably the Herodian bathtub was not made of the 'Bahat' quarried at the Te'omim cave quarry.

The isotopic composition of archaeological artifacts from Herodion, Kotel, Umm el Umdan and N. Natuf fall in the range of the Te'omim cave. It is possible that these artifacts were created from the 'Bahat' quarried at the Te'omim cave quarry. The isotopic composition of speleothems from Abud Cave is characterized by similar $\delta^{18}O$ values, and lower $\delta^{13}C$ values compared with Te'omim cave quarry.

In order to confirm this hypothesis other methods are required in another study.

6 Summary and conclusions

1. TM-2 section was dated from ~1.3 Ma to ~50 ka . U/Th dating of the younger (upper) part, yielded ages between 488ka-53ka, whereas the rest of the section was beyond the limit of U-Th dating method (~500 ka) and was dated by Magneto-stratigraphy and U/Pb. The U/Pb dating gave two ages of 1310 ±60 ka and 1350 ±120 ka, and the magneto stratigraphy of this section gives five ages: 773ka, 1001ka, 1069ka, 1189ka and 1221ka.

Based on these range of dates, the TM-2 $\delta^{18}O$ profile was then dated by "wiggle-matching" its oxygen isotopic record to the globally distributed benthic $\delta^{18}O$ records (Figure 26). Fourteen isotopic events recorded in TM-2 isotopic profile, match MIS events ranging between 1316 ka and 773 ka. The average time period between the $\delta^{18}O$ peaks is about 40ka, matching the 41ka obliquity cycles that occurs until the beginning of the MPT.

The isotopic record of TM-2 reflects a long period of flowstone deposition since almost 1350ka. This record is the longest terrestrial paleoclimatic record at the Mediterranean region.

2. The lower $\delta^{18}O$ values during glacials and interglacial of TM-2 section at the mid Pleistocene transition compared with Soreq cave at the last 230ka indicate a temporal transition of climatic system during the MPT. This difference is also reflected at 40ka cyclicity observed in the TM-2 section that matches the 41ka obliquity cycles that occurred until the beginning of the MPT, compared with the 100ka cyclicity at the late Pleistocene.

Events characterized by low $\delta^{18}O$ associated with high $\delta^{13}C$ values were correlated with sapropel events as was described for Soreq and Jerusalem caves, and may reflect deluge or extremely unstable dry events. During the MPT there is a continuous growth during glacials and interglacials.

3. In general, most of the flowstone section is characterized by large columnar crystals, producing the typical 'Bahat' structure. In some cases, the isotopic trends are associated with significant petrographic textures. (I) High $\delta^{13}C$ and high $\delta^{18}O$ are often characterized by relatively small crystals, though their structure is not uniform. The combination of the isotopic composition of high $\delta^{13}C$ and high $\delta^{18}O$, and the small crystals indicating slow and inconsistent growth, most likely reflecting relatively dry conditions; (II) Low $\delta^{13}C$ and low $\delta^{18}O$ are mostly associated with large, usually not oriented crystals, indicating constant and fast growth, most likely reflecting relatively wet conditions. These wet conditions are not always reflected in the petrographic structure; (III) High $\delta^{13}C$ and low $\delta^{18}O$ peaks are usually associated with homogenous columnar and transparent crystals with preferred orientation. The large and clear calcite crystals reflect constant and more or less homogenous growth due to constant dripping in the cave. (IV) Low $\delta^{13}C$ and high $\delta^{18}O$ values are often characterized by medium-large and clear columnar crystals with preferred orientation, interrupted in places by an area of small crystals. The combination of the isotopic characteristics and the petrography of the calcite crystals may reflect wet and cold climatic conditions, resulting in continuous and constant growth.

4. The isotopic composition of 'Bahat' archaeological artifacts samples from several archeological sites in Israel and Egypt show that most of the 'Bahat' artifacts do not match the $\delta^{13}C$ - $\delta^{18}O$ combination of artifacts imported from Egypt. 'Bahat' artifacts from Umm

el Umdan, Herodion, and Kotel match the isotopic composition of Te'omim Cave and could have been derived from Te'omim quarry. 'Bahat' artifacts from Ceasarea, Tel Yarmuth and Har Habait deviate significantly from both, Egypt and Te'omim isotopic trends. Herodian bathub matches the $\delta^{18}O$ range of Te'omim Cave, with somewhat lower $\delta^{13}C$ values. Additional methods (e.g., trace elements, Sr isotopic composition) are required to find the provenance of 'Bahat' artifacts.

7 References

Almogi-Labin, A., Bar-Matthews, M., & Ayalon, A., 2004. Climate variability in the Levant and northeast Africa during the Late Quaternary based on marine and land records. Human paleoecology in the Levantine corridor, 117-134.

Almogi-Labin, A., Bar-Matthews, M., Shriki, D., Kolosovsky, E., Paterne, M., Schilman, B., & Matthews, A., 2009. Climatic variability during the last~ 90ka of the southern and northern Levantine Basin as evident from marine records and speleothems. Quaternary Science Reviews, 28(25), 2882-2896.

Amir, A., 2016.A Re-Examination of the sources of 'Alabaster' vessels found in archeological exvacations in the land of Israel, following the discovery of an Ancient quarry of Speleothems (calcite alabaster) in Jerusalem hills. Master degree in the Martin (Szusz) department of the land of Israel studies and archeology, Bar Ilan university, Ramat Gan, Israel (Hebrew).

Amiran, R., 1970. The Egyptian alabaster vessels from Ai. Isr. Explor. J. 20 (2),pp. 170-179.

Ayalon, A., Bar-Matthews, M. & Sass, E., 1998. Rainfall-recharge relationships within a karstic terrain in the eastern Mediterranean semi-arid region, Israel: d18O and dD characteristics. Journal of Hydrology, v 207, pp. 18-31.

Ayalon, A., Bar-Matthews, M., Kaufman, A. 1999. Petrography, strontium, barium and uranium concentrations, and strontium and uranium isotope ratios in speleothems as palaeoclimatic proxies: Soreq Cave, Israel. The Holocene 9,pp. 715–722.

Bar-Matthews, M., 2014. History of Water in the Middle East and North Africa. Treatise on Geochemistry, Second Edition, vol. 14.9, pp. 109-124. Oxford: Elsevier.

Bar-Matthews, M., Ayalon, A., Matthews, A., Sass, E., & Halicz, L.,1996. Carbon and oxygen isotope study of the active water-carbonate system in a karstic Mediterranean cave: Implications for paleoclimate research in semiarid regions. Geochimica et Cosmochimica Acta, 60(2), 337-347. Bar-Matthews, M., Ayalon, A., & Kaufman, A. (2000). Timing and hydrological conditions of Sapropel events in the Eastern

Mediterranean, as evident from speleothems, Soreq cave, Israel. Chemical Geology, 169(1), 145-156.

Bar-Matthews, M., Ayalon, A. and Kaufman, A. 1997. Late Quaternary paleoclimate in the eastern Mediterranean region from stable isotope analysis of speleothems at Soreq Cave, Israel. Quaternary Research, 47, 155-168.

Bar-Matthews, M., Ayalon, A. & Kaufman, A., 2000. Timing and hydrological conditions of Sapropel events in the Eastern Mediterranean, as evident from speleothems, Soreq cave, Israel. Chemical Geology, v. 169, pp. 145-156.

Bar-Matthews, M. et al., 2003. Sea-land oxygen isotopic relationships from planktonic foraminifera and speleothems in the Eastern Mediterranean region and their implication for paleorainfall during interglacial intervals. geochimica et cosmochimica, v. 67, pp. 3181-3199.

Ben-Dor, I., 1945. Palestinian alabaster vases. In: Quarterly of the Department of Antiquities of Palestine, 11, pp. 93-112.

Berger, A., & Loutre, M. F., 1991. Insolation values for the climate of the last 10 million years. Quaternary Science Reviews, 10(4), 297-317.

Boistelle, R., 1982. Mineral crystallization from solutions: Estudios Geolo´gicos, v. 38, pp. 135–153.

Bourdon, B., Henderson, G. M., Lundstorm, C. C. & Turner, S. P., 2003. Uranium-series geochemistry. Washington, DC: The Mineralogical Society of America.]

Burton, W.K., Cabrera, N., and Frank, F.C., 1951. The growth of crystals and the equilibrium structure of their surfaces: Royal Society [London], Philosophical Transactions, v. A243, pp.299–358.

Caubet, A., 1991. Répertoire de la vaiselle de pierre: Ougarit 1929-1988. In: Yon, M.(Ed.), Ras Shamra-Ougarit VI: Arts et Industries de la Pierre. Editions Recherches sur les Civilisations, Paris, pp. 205-264.

Clamer, C., 1976. Late Bronze Age alabaster vessels found. In: Palestinian Contexts with an Emphasis on Calcite and Gypsum Tazze. The Hebrew University of Jerusalem, Israel (M.A. thesis).

Clamer, C., 2007. The stone vessels. In: Mazar, A., Mullins, R. (Eds.), Excavations at Tel Beth-Shean 1989-1996, The Middle and Late Bronze Age Strata in Area R, v. II. Israel Exploration Society, Jerusalem, pp. 626e638.

Clark, P. U., Archer, D., Pollard, D., Blum, J. D., Rial, J. A., Brovkin, V., & Roy, M., 2006. The middle Pleistocene transition: characteristics, mechanisms, and implications for long-term changes in atmospheric pCO 2. Quaternary Science Reviews, 25(23), 3150-3184.

Conder, C.R., Kitchener, H.H., 1883. The Survey of Western Palestine: Memoirs. In: Judaea, v. 3. Palestine Exploration Fund, London.

Craig, H, & Craig, V 1972. "Greek marbles: determination of provenance by isotopic analysis." Science 176.4033 (1972): 401-403.

Deines, P. (1980). The isotopic composition of reduced organic carbon. In: Fritz, P., Fontes, J.Ch. (Eds.), Handbook of Environmental Isotope Geochemistry, 1A. Elsevier, Amsterdam, pp. 329-406.

Ebeling, J.R., 2001. Utilitarian Objects in Sacred Spaces: Ground Stone Tools in Middle and Late Bronze Age Temples in the Southern Levant (PhD dissertation). University of Arizona.

Ehleringer, J. R., & Cooper, T. A., 1988. Correlations between carbon isotope ratio and microhabitat in desert plants. Oecologia, 76(4), 562-566.

Emeis, K. C., Schulz, H. M., Struck, U., Sakamoto, T., Doose, H., Erlenkeuser, H., & Paterne, M., 1998. 26. Stable Isotope And Alkenone Temperature Rcords Of Sapropels From Sites 964 And 967: Constraining The Physical Environment Of Sapropel Formation In the Eastern Mediterranean Sea.

Emiliani, C., 1955. "Pleistocene temperatures." The Journal of Geology (1955): 538-578.

Folk, R.L., 1965. Some aspects of recrystallization in ancient limestones, in Pray, L.C., and Murray, R.C., eds., Dolomitization and Limestone Diagenesis: Society of Economic Paleontologists and Mineralogists, Special Publication 13, pp. 14–48.

Ford, D.C., Williams, P.W., 2007. Karst Hydrogeology and Geomorphology. Wiley, Chichester.

Frisia, S., Borasto, A., Fairchild, I.J and Mcdermott, F., 2000. Calcite Fabrics, Growth Mechanisms, And Enviroments Of Formation In Speleothems From The Italian Alps And Southwestern Ireland. Journal Of Sedimantary Research, v. 70, no. 5, , pp. 1183–1196.

Frumkin, A., Fischhendler, I., 2005. Morphometry and distribution of isolated caves as a guide for phreatic and confined paleohydrological conditions. Geomorphology 67, pp. 457-471.

Frumkin, A., Ford, D. C. & Schwarcz, H. P., 1999. Continental oxygen isotopic record of the last 170,000 years in Jerusalem. *Quaternary Research,* Volume 51, pp. 317-327.

Frumkin, A., Ford, D. C. & Schwarcz, H. P., 2000. Paleoclimate and vegetation of the last glacial cycles in Jerusalem from speleothem record. Global Biogeochem Cycles, v. 104, pp. 863-870.

Frumkin, A., Bar-Matthews, M., Davidovich, U., Langford, B., Porat , R., Ullman, M., Zissu, B., 2014. In-situ dating of ancient quarries and the source of flowstone (‘calcite-alabaster’) artifacts in the southern Levant. Journal of Archaeological Science v. 41,pp. 749-758.

Gasse, F., Vidal, L., Van Campo, E., Demory, F., Develle, A. L., Tachikawa, K., & Thouveny, N., 2015. Hydroclimatic changes in northern Levant over the past 400,000 years. Quaternary Science Reviews, 111, 1-8.

Genty, D. & Massault, M., 1999. Carbon transfer dynamics from bomb-14C and d13C time series of a laminated stalagmite from SW France - Modeling and comparison with other stalagmite records. Geochimica et Cosmochimica Acta, 63(10), pp. 1537-1548.

Gonzalez, L., Carpenter, S.J., and Lohmann, K.C., 1992, Inorganic calcite morphology: Roles of fluid chemistry and fluid flow: Journal of Sedimentary Petrology, v. 62, pp. 382–399.

Gorgoni, Carlo, et al.2002. "An updated and detailed mineropetrographic and CO stable isotopic reference database for the main Mediterranean marbles used in antiquity." Asmosia 5 (2002): 115-131.

Grant, K.M., Rohling, E.J., Bar-Matthews, M., Ayalon, A., Medina-Elizalde, M., Bronk Ramsey, C., Satow, C., Roberts, A.P. ,2012. Rapid coupling between ice volume and polar temperature over the past 150 kyr. Nature 491,744-747.

Harrell, J.A., 1995. Ancient Egyptian origins of some common rock names. J. Geol. Edu. 43 (1), pp. 4-30.

Harrell, J.A., Broekmans, M.A.T.M., Godefrey-Smith, D.I., 2007. The origin, destruction and restoration of colour in Egyptian travertine. Archaeometry 49, pp. 421-436.

Hays, J.D., Imbrie, J., Shackleton, N.J., 1976. Variations in the earth's orbit: Pacemaker of the ice ages. Science 194, 1121-1132.

Hendy, C.H., 1971. The isotopic geochemistry of speleothems I. The calculation of the effects of different modes of formation on the isotopic composition of speleothems and their applicability as paleoclimatic indicators: Geochimica et Cosmochimica Acta, v. 35, pp. 801–824.

Hershkovitz, I., Marder, O., Ayalon, A., Bar-Matthews, M., Yasur, G., Boaretto, E., & Gunz, P., 2015. Levantine cranium from Manot Cave (Israel) foreshadows the first European modern humans. Nature, 520(7546), 216-219.

Hertz, N. and Dean, N.E., 1986. "Stable isotopes and archaeological geology: the Carrara marble, northern Italy." Applied Geochemistry 1.1 (1986): 139-151.

Hoek, W. Z., & Bohncke, S. J. P., 2001. Oxygen-isotope wiggle matching as a tool for synchronising ice-core and terrestrial records over Termination 1. Quaternary Science Reviews, 20(11), 1251-1264.

Imbrie, J., Mix, A. C., & Martinson, D. G., 1993. Milankovitch theory viewed from Devils Hole. Nature, 363(6429), 531-533.

Jouzel, J., Masson-Delmotte, V., Cattani, O., Dreyfus, G., Falourd, S., Hoffmann, G., & Fischer, H., 2007. Orbital and millennial Antarctic climate variability over the past 800,000 years. science, 317(5839), 793-796.

Kagan, E.J., Agnon, A., Bar-Matthews, M., Ayalon, A., 2005. Dating large infrequent earthquakes by damaged cave deposits. Geology 33, 261–264

Kallel, N., Paterne, M., Duplessy, J. C., Vergnaudgrazzini, C., Pujol, C., Labeyrie, L., & Pierre, C., 1997. Enhanced rainfall in the Mediterranean region during the last sapropel event. Oceanolica Acta, 20(5), 697-712.

Kaufman, A. Wasserburg, G., Porcelli, D., Bar-Matthews, M., Ayalon, A. and Halicz, L. 1998. U-Th isotope systematics from the Soreq cave, Israel and climatic correlations. Earth and Planetary Science Letters 156, no. 3-4, 141-155. Kaufmann, G., Dreybrodt, W., 2004. Stalagmite growth and palaeo- climate: an inverse approach. Earth and Planetary Science Letters 224, pp. 529–545.

Kaufman, A., 1993. An evaluation of several methods for determining 230ThU ages in impure carbonates. Geochimica et Cosmochimica Acta, 57(10), 2303-2317.

Kim S.-T., and O'Neil, J.R., 1997. Equilibrium and nonequilibrium oxygen isotope effects in synthetic carbonates: Geochimica et Cosmochimica Acta, v. 61, pp. 3461–3475.

Kolodny, Y., Stein, M., Machlus, M., 2004. Sea-rain-lake relation in the Last Glacial East Mediterranean revealed by $\delta^{18}O$ - $\delta^{13}C$ in Lake Lisan aragonites. Geochimica et Cosmochimica Acta, v. 69, No. 16, pp. 4045–4060.

Komintz, M. A., and Pisias N. G., 1979: Pleistocene climate: Deterministic or stochastic? Science,204, 171–172.

Li, H.-C., Ku, T.-H., You, C.-F., Cheng, H., Edwards, R.L., Ma, Z.- B., Tsai, W.-S., Li, M.-D., 2005. $^{87}Sr/^{86}Sr$ and Sr/Ca in speleothems for paleoclimate reconstruction in Central China between 70 and 280 kyr ago. Geochimica et Cosmochimica Acta 69, pp. 3933–3947.

Lilyquist, C.,1996. Stone vessels at Kamid el-Loz, Lebanon: Egyptian, Egyptianizing, or Non-Egyptian? A Question at Sites fromthe Sudan to Iraq to the Greek Mainland. In: Hachmann, R. (Ed.), Kamid el-Loz 16. 'Schatzhaus'-Studien, Saarbruecker Beitraege zur Altertumskunde, v. 59. R. Habelt., Bonn, pp. 133-173.

Lisiecki, L. and Raymo, M., 2005. "A Pliocene-Pleistocene stack of 57 globally distributed benthic δ18O records." Paleoceanography 20.1 (2005).

Lucas, A., 1930. Egyptian Predynastic stone vessels. J. Egypt Archaeol. 16 (3-4), pp. 200-212.

Lüthi, D., Le Floch, M., Bereiter, B., Blunier, T., Barnola, J. M., Siegenthaler, U., & Stocker, T. F. ,2008. High-resolution carbon dioxide concentration record 650,000–800,000 years before present. Nature, 453(7193), 379-382.

Manfra, L., U. Masi, and B. Turi. "Carbon and oxygen isotope ratios of marbles from some ancient quarries of western Anatolia and their archaeological significance." Archaeometry 17.2 (1975): 215-219.

Mann, G., 1978. On a rope-to the pit in the Te'omim Cave. Teva va-Aretz 20, pp. 161-164 (Hebrew).

Martinson, D. G., Pisias, N. G., Hays, J. D., Imbrie, J., Moore, T. C., & Shackleton, N. J., 1987. Age dating and the orbital theory of the ice ages: development of a high-resolution 0 to 300,000-year chronostratigraphy. Quaternary research, 27(1), 1-29.

Mcdermott, F., 2004. Palaeo-climate reconstruction from stable isotopic variations in speleothems: a review. Quaternary Science Reviews, 23(7-8), pp. 901-918.

Neuville, R., 1930. Notes de Préhistoire Palestinienne; La Grotte d'et-Taouamin. J. Palest. Orient. Soc. 10, pp. 64-75.

Prell, W. L., Imbrie, J., Martinson, D. G., Morley, J. J., Pisias, N. G., Shackleton, N. J., & Streeter, H. F., 1986. Graphic correlation of oxygen isotope stratigraphy application to the late Quaternary. Paleoceanography, 1(2), 137-162.

Press, M.D., 2011. Faience and alabaster vessels (Chapter 14). In: Stager, L.E., Master, D.M., Schloen, J.D. (Eds.), Ashkelon 3, the Seventh Century B.C. Eisenbrauns, Indiana, pp. 421-429.

Prieto, M., Garcia-Ruiz, J.M., and Amoro's, J.L., 1981. Growth of calcite crystals with nonsingular faces: Journal of Crystal Growth, v. 52, pp. 864–867.

Quade, J., Cerling, T. E., & Bowman, J. R., 1989. Systematic variations in the carbon and oxygen isotopic composition of pedogenic carbonate along elevation transects in the southern Great Basin, United States. Geological Society of America Bulletin, 101(4), 464-475.

Richards, D. A. & Dorale, J. A., 2003. Uranium-series chronology and environmental applications of speleothems. Reviews in mineralogy and geochemistry, v. 52, pp. 407-460.

Shackleton, N. J., and Opdyke N.D., 1973. "Oxygen isotope and palaeomagnetic stratigraphy of equatorial Pacific core V28-238: Oxygen isotope temperatures and ice volumes on a 10 5 year and 10 6 year scale." Quaternary research 3.1, 39-55.

Singer, B. S. (2014). A quaternary geomagnetic instability time scale. Quat. Geochronol. 21, 29-52.

Smith, B.N. and Epstein, S., 1971. two categories of $^{13}C/^{12}C$ ratios for plant. Plant Physiol., 47, 380-384.

Sosdian, S., & Rosenthal, Y., 2010. Response to Comment on "Deep-sea temperature and ice volume changes across the Pliocene-Pleistocene climate transitions". Science, 328(5985), 1480-1480.

Sparks, R., 2007. Stone Vessels in the Levant, the Palestine Exploration Fund Annual VIII. Maney, Leeds.

Stepanov, V.I., 1997, Notes on mineral growth from the archive of V.I. Stepanov (1924–1988) translated by V.N. Koulanin: University of Bristol, Spelaeological Society, Proceedings, v. 21, pp. 25–42.

Sunagawa, I., 1987, Morphology of minerals, in Sunagawa, I., ed., Morphology of Crystals:Tokyo, Terra Scientific Publishing Company, pp. 509–587.

Szabo, B.J., Kolesar, P.T., Riggs, A.C., Winograd, I.J., and Ludwig, K.R., 1994. Paleoclimatic inferences from a 120,000-yr calcite record of water-table fluctuation in Browns Room of Devils Hole, Nevada: Quaternary Research, v. 41, pp. 59–69.

Tieszen, L. L., 1991. Natural variations in the carbon isotope values of plants: implications for archaeology, ecology, and paleoecology. Journal of Archaeological Science, 18(3), 227-248.

Ussishkin, D., 1980. The Ghassulian shrine at Ein Gedi. Tel Aviv 7 (1), pp. 1-44.

Vaks, A., Bar-Matthews, M., Matthews, A., Ayalon, A., & Frumkin, A. (2010). Middle-Late Quaternary paleoclimate of northern margins of the Saharan-Arabian Desert: reconstruction from speleothems of Negev Desert, Israel. Quaternary Science Reviews, 29(19)

Vaks, A., Bar-Matthews, M., Ayalon, A., Matthews, A., Frumkin, A., Dayan, U., & Schilman, B., 2006. Paleoclimate and location of the border between Mediterranean

climate region and the Saharo–Arabian Desert as revealed by speleothems from the northern Negev Desert, Israel. Earth and Planetary Science Letters, 249(3), 384-399., 2647-2662.

Zissu, B., Porat, R., Langford, B., and Frumkin, A., 2011. Archaeological Remains of the Bar Kokhba Revolt in the Te'omim Cave (Mŭghâret Umm et Tûeimîn), Western Jerusalem Hills. Journal of Jewish Studies 52,2, 262-283.

Appendix 1

$\delta^{18}O$ and $\delta^{13}C$ values of Bahat samples

Item	$\delta^{13}C$ (‰ VPDB)	$\delta^{18}O$ (‰ VPDB)
Amid-3-Nahal Natuf	-10.54	-4.71
Amid-4-Kotel	-10.95	-6.45
Amid-6-Um el umdan	-10.14	-5.48
Amid-16-Egypt	-8.45	-10.13
Amid-17-Egypt	-6.62	-8.35
Amid-20--Egypt	-7.3	-11.67
Amid-23-Har Habait	3.73	-8.87
Amid-27-Egypt, modern	-8.2	-9.56
Amid-30-Teomim cave	-5.62	-6.71
Amid-31-Herodion	-10.17	-4.07
Amid-32-Herodion	-10.17	-4.86
Amid-33-Abud Cave	-11.25	-5.55
Amid 25--40081-Har Habait	4.06	-7.16
Amid-7-8-Umm el umdan	-10.98	-6.67
Amid-50-Bizant	0.08	-9.57
Amid 49- modern Egypt	-5.23	-6.84
Amid-Te 25-Teomim cave	-10.35	-7.54
Amid 50-Ceasarea	-0.31	-9.14
Amid 52- Tel Yarmuth	-1.2	-8.57
Amid - 51- k41738-Hordus Bath	-12.8	-5.07
Amid - 51- k41738-Hordus Bath	-12.74	-4.62
Amid - 51- k41738-Hordus Bath	-12.75	-4.72

Description of Bahat samples (Translated from Amir, 2016)

Sample no. 25 The quarry wall at Te'omim Cave	Sample no. 3 Speleothem from Nahal Natuf Cave
	
Sample no. 4 Pillar from the Kotel Excavations, Jerusalem 	Sample no. 5,6 Chips from Umm el Umdan Site number 58. 1-6/3 (Weiss at al, 2005). 

Sample no. 7,8 Bahat bloc from Umm el Umdan Site number 58. 1-6/3 (Weiss at al, 2005).  	Sample no. 7,8 Bahat bloc from Umm el Umdan Site number 58. 1-6/3 (Weiss at al, 2005). 
Sample no. 16,17,20 Bahat archeological artifacts fragments (ancient), Giza, Egypt. The Austrian delegation to Egypt, the 19# century.	Sample no. 23, 25 Marble artifact fragments, Har Habait (Jerusalem)

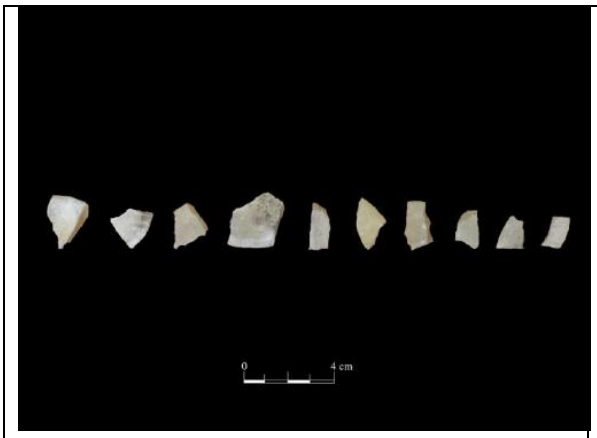

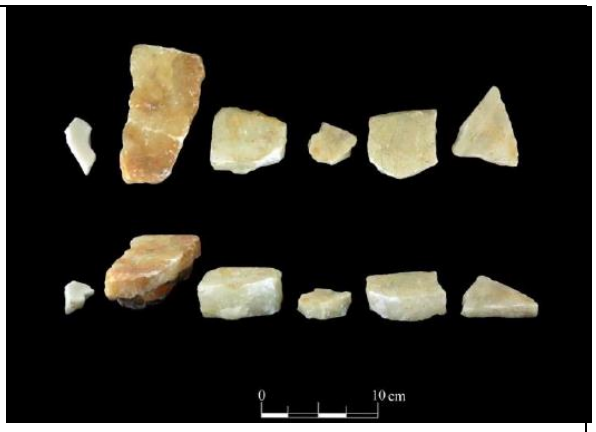

Sample no. 27

Bahat bloc (modern), Cairo, Egypt.

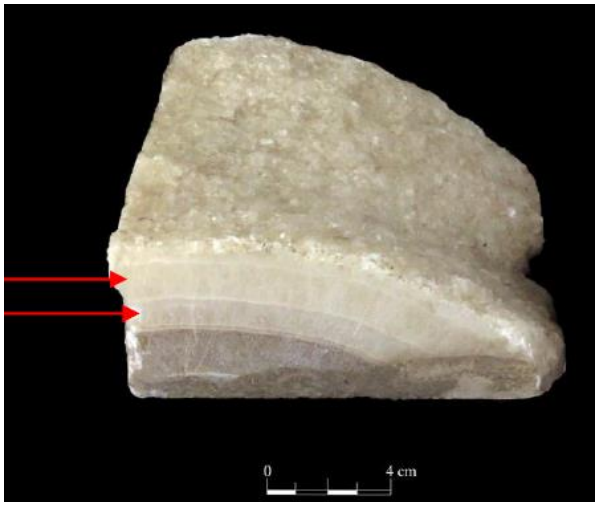

Sample no. 30

Archeological artifact fragment, Te'omim cave.

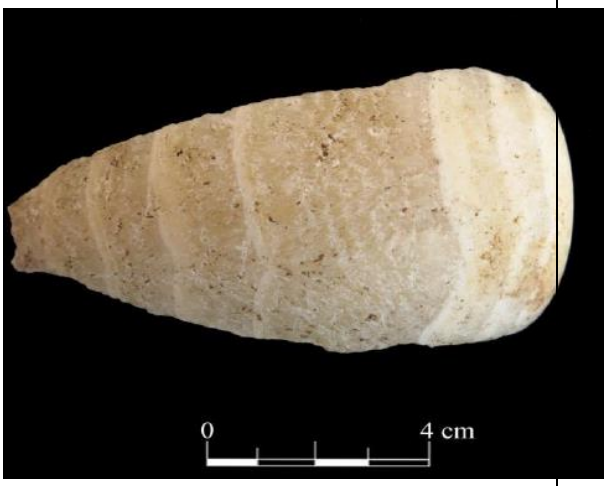

Sample no. 31,32

A basin side wall, Herodion

Sample no. 33

Quarry wall, Abud cave


0
4 cm


0
10 cm

Sample no. 49

Modern vessel, Egypt.

Sample no. 51

Herodian Bath, Cypros.

Sample no. 52

Bowl fragment, Tel Yarmuth.

ו-1221 אלף שנה. הרקורד האיזוטופי של TM-2 מייצג תקופה ארוכה של השקעת משטחי זרימה מלפני כ-1350 אלף שנה. מדובר ברקורד הפליאואקלימי היבשתי הארוך ביותר באזור הים תיכוני.

אירועי ספרופל אופיינו בחתך באמצעות $\delta^{18}O_c$ נמוך ו-$\delta^{13}C$ גבוה יחד עם עריכת 'wiggle mathcing' (התאמה גרפית) של הפרופיל האיזוטופי עם הרקורד האיזוטופי LR04 של $\delta^{18}O_c$ של פורומיניפרים בנטוניים. 14 אירועים שזוהו בפרופיל האיזוטופי של TM-2 הותאמו לאירועי MIS בטווח של 1316 אלף שנה עד 773 אלף שנה. תקופת הזמן הממוצעת בין השיאים העיקריים של $\delta^{18}O$ הינה כ-40 אלף שנה, אשר תואמת למחזוריות של נטיית ציר הסיבוב של כדור הארץ (obliquity) שהתקיימה עד לתחילת תקופת מעבר אמצע הפלייסטוקן, MPT (כ-700 אלף שנה).

בתקופת הפלייסטוקן התחתון, ישנו גידול רציף במהלך תקופות גלציאל ואינטרגלציאל. ערכי $\delta^{18}O$ של TM-2 במהלך הפלייסטוקן התחתון בתקופות גלציאל ואינטרגלציאל נמוכים בהשוואה לערכים שנמדדו במערת שורק ב-230 אלף השנים האחרונות, מה שמעיד על על מערכת אקלימית שונה. אירועים המאופיינים בערכים נמוכים של $\delta^{18}O$ ביחד עם ערכים גבוהים של $\delta^{13}C$ קשורים באירועי ספרופל כפי שתואר במערות שורק וירושלים ויתכן ומעידים על אירועים שטפוניים.

שלושה עשר שקפים נוסרו מהחתך TM-2 ונחקרו באמצעות מיקרוסקופ אופטי מקטב על מנת לאפיין את אופי ותבנית גידול הגבישים. רוב החתך מאופיין בגבישים גדולים, מאורכים המספקים סטרוקטורה אופיינית לבהט. בחלק מהמקרים, המגמות האיזוטופיות קשורות בטקסטורות פטרוגרפיות משמעותיות.

הרכבים איזוטופיים של חמצן ופחמן של כלי בהט ממצרים וישראל נמדדו על מנת להשוות אותם לערכים האיזוטופיים של TM-2 במטרה להוסיף מידע על מקורם של הכלים. ההרכב האיזוטופי של הכלים מאתרים ארכיאולוגיים בישראל מראה כי רוב הכלים לא מתאימים להרכבים האיזוטופיים של הכלים שיובאו ממצרים. ההרכב האיזוטופי של כלי בהט מאום אל עומדן, ההרודיון והכותל מתאים להרכב האיזוטופי של מערת התאומים ויתכן ומקורם במחצבה שבמערה. נדרשות שיטות נוספות (כגון איזוטופים של סטרונציום ויסודות קורט) על מנת לאתר באופן מובהק יותר את מקור הכלים.

תקציר

מערת התאומים היא מערת המסה קארסטית הממוקמת במדרונות המערביים של הרי ירושלים, כ-20 ק״מ מערבית לירושלים בנחל המערה (נ.צ. 202049/726028). במערה נמצא טווח רחב של ספלאותמים ואדוסים כגון משטחי זרימה, נטיפים וזקיפים שהושקעו בחלקים שונים בחלל המרכזי של המערה, כאשר חלקם יצרו חתך עבה של משטחי זרימה וזקיפים. במחקר עדכני שנערך במערה, אותרה מחצבה בחלק המזרחי של החלל המרכזי במערה. המחצבה תוארכה בשיטת אורניום-תוריום באמצעות תיארוך של משטחי זרימה שהושקעו מעל משטח החציבה לאחר תום החציבה, והגיל שהתקבל הינו תקופת הברונזה התיכונה (לפני כ-3500 שנה). החומר שנחצב מורכב ממשטחי זרימה המורכבים משכבות גבישי קלציט גדולים ובעלי שקיפות שככל הנראה שימשו בעבר כמקור ל׳בהט׳ (קלציט אלבסטר). המונח ׳בהט׳ משמש בספרות הארכיאולוגית העברית המודרנית להגדרת קלציט אלבסטר. בעבר נהוג היה לחשוב כי חפצים המורכבים מקלציט אלבסטר אשר נמצאו בדרום הלבנט יובאו ממצרים. ההנחה שאין אפשרות למקור מקומי לקלציט אלבסטר התקבלה לפני שנים רבות, ובהתאם לכך רוב המחקרים הניחו שמקורם של החפצים במצרים. בניגוד לכך הסתבר כי מחצבות של קלציט אלבסטר אכן קיימות בדרום הלבנט לפחות בשתי מערות, מערת התאומים ומערת עבוד, וככל הנראה מחצבות אלו היוו מקור מקומי אלטרנטיבי לחומר היוקרתי.

חתך של משטחי זרימה בעובי של כ-3 מ׳, TM-2, נדגם מקיר המחצבה. המיקום נבחר היכן שנמצא חתך בעל עובי מקסימלי של משטחי זרימה נקיים על מנת לאפיין את החתך העיקרי במחצבה. שמונים הס״מ העליונים של TM-2, נחקרו בעבודה זו.

דגימות למדידת ערכי $\delta^{18}O_c$ ו-$\delta^{13}C$ נלקחו במרווחים של כ- 0.5-1.0 מ״מ (459 דגימות נקדחו בחתך TM-2), לשם תיארוך ושחזור שינויים אקלימיים וסביבתיים. עשרת הס״מ העליונים של החתך תוארכו תחילה באמצעות שיטת אורניום- תוריום. החלק העתיק יותר של החתך תוארך באמצעות שיטת אורניום- עופרת ובאמצעות פליאומגנטיזם. החתך תוארך לתקופה שבין כ-1300 אלף שנה עד לכ-50 אלף שנה. בשיטת האורניום-עופרת התקבלו שני גילים, 1310 ± 60 אלף שנה ו-1350 ± 120 אלף שנה ובשיטת המגנטוסטרטיגפיה התקבלו חמישה גילים: 773, 1001, 1069, 1189

המכון הגיאולוגי
משרד התשתיות הלאומיות
האנרגיה והמים

משטחי זרימה במערת התאומים, ישראל: מאפיינים ומגמות אקלימיות בתקופת המעבר הפליסטוקנית MPT

יעל אמיד

עבודה זו הוגשה כחיבור לקבלת תואר "מוסמך" באוניברסיטה העברית בירושלים.

העבודה נעשתה בהדרכתם של:

ד"ר מירה בר-מטיוס, המכון הגיאולוגי, ירושלים.

פרופ' עמוס פרומקין, המרכז לחקר מערות, האוניברסיטה העברית בירושלים.

דוח מס' GSI/39/2016 ירושלים, כסלו תשע"ז, דצמבר 2016